Evaluation of a High-Resolution Regional Climate Simulation for Surface and Hub-height Wind Climatology over North America

Kyle Peco[1], Jiali Wang[1], Chunyong Jung[1], Gökhan Sever[1], Lindsay Sheridan[2], Jeremy Feinstein[1], Rao Kotamarthi[1], Caroline Draxl[3a], Ethan Young[3], Avi Purkayastha[3], and Andrew Kumler[3]

[1]Environmental Science Division, Argonne National Laboratory, Lemont, IL, 60439, United States
[2]Pacific Northwest National Laboratory, Richland, Washington, 99354, United States
[3]National Renewable Energy Laboratory, Golden, Colorado, 80401, United States
[a]Now at Electric Power Research Institute, Palo Alto, California, 94304, United States

Correspondence to: Kyle Peco (kpeco@anl.gov) and Jiali Wang (jialiwang@anl.gov)

Abstract. Assessing the availability of key wind resources requires augmenting observations to support the implementation of wind energy infrastructure. However, observations are limited, necessitating the development of high resolution, long-term gridded datasets. This study presents a robust, dynamically downscaled climatological dataset, offering 20 years of hourly wind data at a 4-km spatial resolution across North America, and evaluates its performance against observations, including meteorological towers and Automated Surface Observing Stations (ASOS), as well as a coarse-resolution reanalysis data — European Centre for Medium-Range Weather Forecasts (ECMWF) reanalysis version 5 (ERA5). Results demonstrate that the downscaled high resolution wind data outperforms ERA5 in regions of complex terrain and coastal areas, with improved overlap coefficients for wind data distributions and reduced root mean square errors (RMSE) for hub-height and near-surface diurnal wind patterns. The downscaled simulation also reasonably captures the synoptic drivers of seasonal wind direction patterns, indicated by high wind rose similarity indices. This study also provides an analysis of interannual variability, utilizing the dataset's full 20-year period, and model uncertainty, generated by varying model initial conditions and physics parameterizations across 1-year ensemble members, which are key considerations for wind resource assessment in wind farm development.

1 Introduction

Wind is a key factor in shaping a region's complex climate, influencing both environmental and economic sectors. Understanding local and regional wind variability is vital for assessing wind energy potential, which aids in the efficient implementation and operation of wind farms (Millstein et al., 2019; Couto & Estanquiero, 2021). Additionally, evaluating wind speed and direction is essential for conducting accurate climatological assessments to determine the long-term changes in regional wind patterns. However, the spatiotemporal coverage of current wind measurements remains very limited, particularly over complex terrains (e.g., western US), offshore, and at hub-heights, where wind energy resource assessments are crucial.

To bridge the gap between limited observational data and the need for accurate wind resource assessments, global and regional reanalysis datasets, such as Modern-Era Retrospective analysis for Research and Applications version 2 (MERRA-2), the North American Regional Reanalysis (NARR), and the European Centre for Medium-Range Weather Forecasts Reanalysis version 5 (ERA5), are commonly used (Hersbach et al., 2020; Gelaro et al., 2017; Mesinger et al., 2006). These reanalysis datasets provide valuable insights into wind patterns, variability, and long-term trends, and are also crucial for capturing climatological oscillations and large-scale circulations that influence wind characteristics (e.g., Sheridan et al., 2022a). While these datasets typically have higher horizontal resolution than global climate models (GCMs), they still lack the resolution necessary to explicitly resolve convection and represent fine-scale surface variations, which is essential for capturing convectively driven precipitation and wind (Murakami, 2014; Jones et al., 2021). Additionally, validating these reanalysis datasets is essential for determining their viability for wind resource assessments. (Sheridan et al., 2020, 2024; Lee et al., 2014). For example, Sheridan et al. (2022b) found that ERA5 generally underestimates wind speed diurnal cycles based on 62 sites at a variety of heights above ground across the continental United States (CONUS). This underestimation is most prominent in late afternoon, caused primarily by the underestimation of convectively driven strong winds. Similarly, Chen at al. (2024) and Wilczak et al. (2024) found that ERA5 showed significant negative biases for wind speeds in areas of complex terrain, especially over the Rocky Mountains.

To achieve the necessary high resolution to capture finer scale wind patterns over large spatial areas and extended time periods, researchers employ a technique called dynamical downscaling. This technique involves using initial and boundary conditions from the global or regional reanalysis data to force simulations at finer resolutions using a regional climate model. Regional climate modeling at a convection-permitting (CP) resolution, with a horizontal grid spacing of less than approximately 4 km, has become a promising approach for delivering more reliable climate information at regional and local levels. By directly resolving deep convective processes rather than relying on parameterization, these models demonstrate significant enhancements (e.g., Prein et al., 2015 and the references therein). Due to recent breakthroughs in computational capacity and data management, several studies have been able to perform convection-permitting regional climate model (RCM) simulations. These simulations, especially those concentrating on the CONUS, (e.g., Draxl et al., 2015b; Gensini et al., 2022, Liu et al., 2017; Rasmussen et al., 2024) have shown substantial progress in depicting precipitation, wind, and high-impact weather from national to regional spatial scales. Among these, Draxl et al. (2015a, b) presented the largest, freely available wind dataset at the time of its development, serving the Wind Integration National Dataset (WIND) Toolkit for wind resource assessment and grid integration studies. The data provides time series of meteorological variables every 5 min and 2km across the CONUS in the 7 years from 2007 to 2013.

This study builds upon previous efforts by presenting an additional high-resolution, long-term dataset, along with ensemble simulations for quantifying model uncertainty, for utilization in climatological wind assessments. The dataset was generated by a regional climate model using the Weather Research and Forecasting (WRF) model. With 4 km, 20-year, hourly output, and a model domain spanning the majority of North America and surrounding oceans, this dataset provides a spatiotemporal extension to existing climatological wind analyses. With large geographic coverage, this data product also offers insight into more remote, topographically complex regions, potentially highlighting viable areas for wind energy outside of CONUS. By leveraging a single large spatial domain, the model evolved as one system, developing its own natural variability without being constrained by the forcing data. This dataset has been leveraged by the latest WIND Toolkit Long-term Ensemble Dataset (WTK-LED), as documented by Draxl et al. (2024), serving as the WTK-LED Climate dataset (Table ES-1 in Draxl et al. 2024). Ultimately, this high-resolution dataset aims to combine the climatological significance of an extensive temporal length with the wind-resource-utility advantages of a large spatial domain.

Our study validates the dynamically downscaled model wind speeds and wind directions against various observational data at both the near-surface and at turbine-heights at mostly inland and onshore locations, investigating model performance at different temporal scales (diurnal, seasonal, interannual variability). Especially in the context of wind energy, both speed and direction are crucial components to consider when maximizing the efficacy and operability of wind farms, as speed largely determines the amount of power generated while direction can incite microscale differences in wake effects. A complementary study evaluating the same dataset but focusing on CONUS coastal areas has been documented by Sheridan et al. (2024). Our validation is also performed on the forcing data - ERA5 reanalysis (Hersbach et al., 2020), aiming to understand the added value of the dynamically downscaled model to its coarser resolution forcing data. Additionally, this study seeks to augment insights on model uncertainty within wind simulations that are brought about by varying model configurations.

This manuscript is organized in the following structure: the methodology, including model description, observational datasets used for validation, and analysis metrics used for evaluation are outlined in Section 2. The results of the model's performance at hub-heights and near surface are presented in Section 3.1 and 3.2, with an exploration of model bias in Section 3.3. Interannual variability and model uncertainty are quantified in Section 3.4 with the context of wind energy implications. Lastly, a summary of our findings and avenues for future research are discussed in Section 4.

2 Methods and Datasets

2.1 Model Setup

The wind validation performed in this study was based on a 20-year (2001-2020) climatological dataset produced by the WRF model (Powers et al., 2017) version 4.2.1 with the Advanced Research WRF dynamic core (Skamarock & Klemp, 2008): the Argonne Downscaled Data Archive version 2 (ADDA-v2). With a domain of 2050 x 1750 grid points at a 4-km grid spacing

(8200 km x 7000 km), the model featured over 3.5 million grid cells, horizontally spanning across the majority of North America and the Caribbean Islands (Fig. 1a in Akinsanola et al., 2024). The model was run with 50 unevenly spaced sigma levels, 18 of which were within the lowest 1km (8, 25, 42, 58, 75, 104, 147, 189, 231, 274, 317, 360, 403, 468, 555, 643, 777, and 957m above ground level), and 10 of them are below 300m above the ground to ensure the hub-height winds are calculated directly by the model. Initial and lateral boundary conditions were determined by ERA5. The model was reinitialized for each year on November 1, ultimately producing a series of 20, 14-month simulations covering the period from 2001-2020. The first two months (November and December) of each year were discarded as spin-time time and not used for the data analysis. The reinitialization approach was chosen since the RCM was driven by high-resolution reanalysis data, instead of coarse resolution GCMs which usually require at least one year of spin up time. While soil moisture is typically a concern when reinitializing models during the cold months, the soil moisture of both the ERA5 forcing data and ADDA-v2 was validated and found to be realistic (Akinsanola et al., 2024).

The Yonsei University (YSU) PBL scheme was used for these simulations, which runs with topographic correction for surface winds (topo_wind=1 WRF; Jiménez & Dudhia, 2012; Skamarock et al., 2019) to represent extra drag from subgrid topography and enhanced flow at hilltops. The surface layer scheme used was the MM5 similarity scheme, which follows the Monin-Obukhov similarity theory (Monin & Obukhov, 1954) alongside the Carlson-Boland similarity functions (Carlson and Boland, 1978). The Unified Noah land-surface model was used for the land surface processes, which employs a 4-layer soil temperature and moisture scheme, as well as fractional snow cover and frozen soil physics (Tewari et al., 2004). A full list of model parameterizations can be found in Table 1. No internal grid nudging nor spectral nudging was employed for these simulations because it requires additional computational resources (20-30% more for our configuration), and the ERA5 forcing data is at a relatively higher resolution than other reanalysis datasets, which can provide good boundary conditions and allow the model to develop its own spatiotemporal variability. Model output data for the most used meteorological variables, such as air temperature, wind speed and direction, and precipitation, were saved at hourly intervals for the full domain from 2001-2020. Other variables less frequently used were saved at 3-hour intervals.

2.2 Model Uncertainty

There are multiple sources of model uncertainty in regional weather and climate models (Hawkins & Sutton, 2009). The dominant uncertainty for near-term simulations includes model internal variability and structure uncertainty. The internal variability is caused by varying initial conditions, while structure uncertainty is generated by various physics parameterizations. To study the model's internal variability, we conducted ten additional 1-year (ENSO neutral year - 2018) ensemble runs, all with the same model setup as described in Section 2.1, but different initial conditions (Wang et al., 2018). This was achieved by running each of the ten ensemble members 12 hours apart, with the first being initialized on November 1, 2017, at 00 UTC and the last being initialized on November 5, 2017, at 12 UTC. Thus, the slightly different initial conditions at each respective start time acted as the catalyst to generate differences between the ensemble members. The number of internal variability ensembles was chosen based on the logic of Wang et al. (2017), which demonstrated that 10 ensemble members with varying initialization times was the minimum number needed to capture the internal variability of the model.

To investigate the model's structure uncertainty arising from important physics parameterizations for wind, namely the PBL and land surface model (LSM), an additional six ensemble members were generated for the same neutral year 2018. Each ensemble member shared the same domain and spatial resolution but employed two different and widely used PBL schemes (YSU and MYNN) and LSMs (Noah and NoahMP) for wind energy applications (Draxl et al., 2014; Yang et al., 2017). The MYNN PBL scheme is a level 2.5 closure scheme for turbulence and implicitly solves for turbulence using parametric equations. It gives estimates of TKE and dissipation rates within the boundary layer of the atmosphere (Nakanishi & Niino, 2009). Noah-MP is an improved version of the Noah LSM and provides better representations of terrestrial biophysical and hydrological processes (Niu et al., 2011). A major physical mechanism enhancement includes improved treatment of soil moisture. Two dynamic vegetation options and two surface layer drag coefficient calculation options were also perturbed within the Noah-MP LSM. Thus, in total we had ten combinations with five LSM options and two PBL options. We experimented with these ten runs for a subregion over Southern Great Plains (with various topographic characteristics) and determined that six of the ten runs were able to capture the range of model uncertainty across the domain. Then, we used these six representative combinations for the entire North American domain and entire year of 2018. While the 16 ensemble members do not capture all model uncertainty, they do represent a robust range of model variability due to these perturbations in initial conditions and key physics parameterizations (see more details in Draxl et al., 2024).

Table 1: WRF model setup and ensemble runs used in ADDA_v2 simulations

Regional Climate Model	WRF v4.2.1
Initial and Boundary Conditions	ERA5 at 0.25 deg, every 3 hours
Horizontal Grid Spacing and Timesteps	4km; adaptive time stepping
Number of Grid Cells	2050 (west-to-east) x 1750 (south-to-north) x 49 (top-to-bottom)
Simulation Period	January 1, 2001, to December 31, 2020
Microphysics Scheme	Morrison double moment (Morrison et al., 2005)
Land Surface Scheme	Unified Noah (Tewari et al., 2004), Noah-MultiParameterization (NoahMP, Niu et al., 2011) with two options for dynamic vegetation and surface
Planetary Boundary Layer Scheme	Yonnsei University (Hong et al., 2006), Mellor-Yamada-Nakanishi-Niino (MYNN, Nakanishi & Niino, 2009)
Short and Long-wave Radiation Scheme	Rapid Radiative Transfer Model for GCMs (RRTMG; Iacono et al., 2008)

2.3 Observational Datasets Used for Validation

The validation performed on ADDA-v2 used wind speed observational data taken within 100 meters above ground level. The first collection of observations focused on hub-height wind speeds and wind directions. These observations were taken from multiple meteorological towers hosted by the US Department of Energy National Laboratories (Argonne National Laboratory, Brookhaven National Laboratory, NREL, Oak Ridge National Laboratory, Pacific Northwest National Laboratory, Savannah River National Laboratory), and the National Oceanic and Atmospheric Administration (National Centers for Environmental Information, National Data Buoy Center). In total, 26 meteorological towers were sampled and quality controlled for this analysis, with wind speed observations taken anywhere from 10m to 100m above ground level. Observations were quality controlled through the process of removing atypical or unphysical reported wind speeds (less than 0 m s^{-1}, greater than 50 m s^{-1}, or non-varying values over periods of time greater than 3h), based on Sheridan et al. (2024). Mast flow distortion corrections were not implemented since most locations had only one anemometer reading. For sites with multiple anemometer readings, instrumentation metadata, such as anemometer orientation with respect to nearby structures, was not included, and we did not want to make corrective assumptions. While different factors, such as instrument precision, environmental effects such as land use, obstructions, or elevation effects, and the temporal sampling methods can introduce uncertainty into the collected observational wind, the quality control procedures conducted here maximize the integrity and reliability of the data used for this validation.

Temporal coverage for the meteorological towers varied between 2-20 years, with an average of ~8.1 years. Observations covered a diverse range of geographies, including mountainous, coastal (east and west coast of the CONUS), the Great Lakes, and plains regions; Alaska and Puerto Rico (Caribbean) were denoted as separate geographic regions. For 19 of these meteorological towers, the exact locations, anemometer heights, and temporal coverages of wind observations can be found in Table 2. The remaining 7 are proprietary data, in which exact locations could not be specified. While turbine-height wind speed and wind direction data are sparse, we have leveraged all the publicly available resources that we have access to and performed a thorough validation over diverse geospatial areas.

The second part of this evaluation explores an expansive collection of 10 m wind speed data sourced from a network of Automated Surface Observing Stations (ASOS). These stations monitor and report various meteorological variables and are operated by the United States National Weather Service, the Federal Aviation Administration, and the Department of Defense. The specific dataset used for this validation was collected from the Iowa Environmental Mesonet (IEM) and subsequently quality controlled by the Data Archive and Portal (DAP) Platform. The dataset hosts over 2,000 sites across CONUS and Alaska and covers a temporal period from 1 January 2000 – 31 December 2021, offering a spatiotemporally comprehensive means for performing a thorough validation of ADDA-v2's 10m wind. Additionally, wind speed data from four additional ASOS stations over Puerto Rico were downloaded from the Iowa Environmental Mesonet (IEM) to spatially

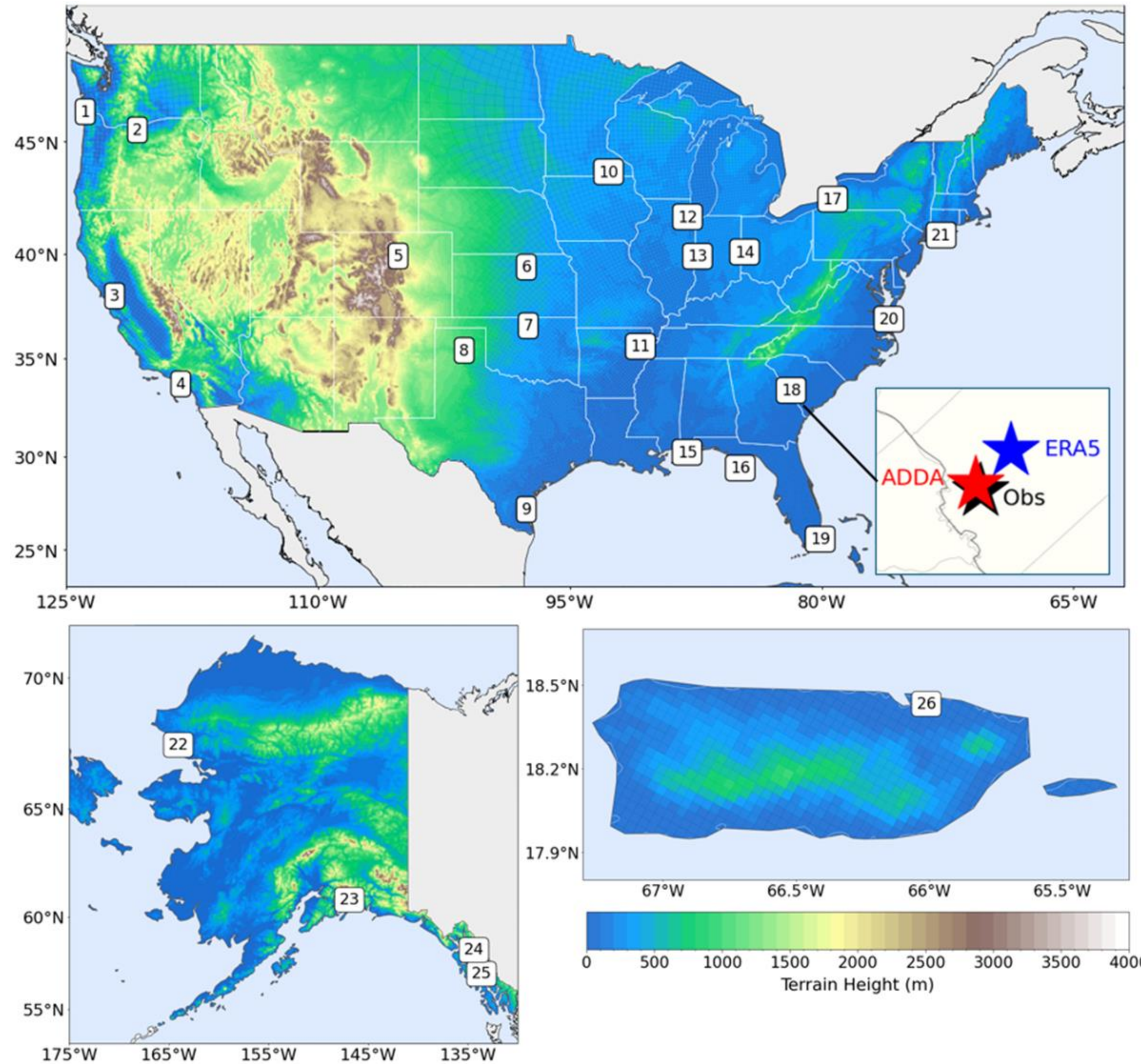

Figure 1. Locations of in-situ observations sampled from meteorological towers across CONUS and Alaska, along with an ASOS location over Puerto Rico. The zoomed in area, with stars representing each dataset, indicates the capability of ADDA-v2's higher resolution to more closely match the exact location of the in-situ data. The 2000+ sites over CONUS are not included here but can be seen in Fig. 6.

expand the model validation and gain a more comprehensive understanding of model performance over areas of sparse data availability and complex terrain.

To demonstrate the potential added value of ADDA-v2 to its coarse resolution forcing data, we also included ERA5 reanalysis in all near-surface and hub-height evaluations. ERA5 outputs only two levels of wind (10m and 100m), so to evaluate winds at heights between these levels, an interpolation method was required. At each timestamp, the ADDA-v2 and ERA5 wind speeds were adjusted to the observational heights via the power law using the model wind speeds at surrounding output heights to the observation height. While this interpolation method may induce some bias in both ADDA-v2 and ERA5, the differences between these datasets are driven mostly by the difference in spatial resolution and the added value by ADDA-v2. This approach was selected based on the analysis of Duplyakin et al. (2021), who found that the power law minimized errors due to vertical adjustment of wind dataset output heights to observation heights.

2.4 Statistics for Validation

The wind speed validation in this study utilizes several statistical error metrics to evaluate how well ADDA-v2 performs against observations. Root mean square error (RMSE), Pearson correlation coefficients (r), overlap coefficients (OVLs), and wind rose similarity indices (WRSIs) are used.

The RMSE gives a metric for the overall accuracy of the model, with lower RMSE's indicating improved model performance. RMSE is taken as the square root of the average of the squared differences between simulated wind speeds and the observed wind speeds at various timescales (seasonal, monthly, diurnal), given by Eq. (1). This metric is effective at highlighting instances of larger errors in the model and demonstrates the overall magnitude of model inaccuracy. Here, $\boldsymbol{n}$ represents the number of wind speed observations (in time), $\boldsymbol{v}_{\mathbf{mod}}$ represents the modeled wind speed, and $\boldsymbol{v}_{\mathbf{obs}}$ denotes the observed wind speed. Relative RMSE (rRMSE) was also considered, Eq. (2), by dividing the RMSE by the average of the observed wind speed. This gives a general sense of the magnitude of error in relation to the magnitude of the wind speeds themselves.

$$\mathrm{RMSE} = \sqrt{\frac{1}{n}\sum_{i=0}^{n}(v_{\mathrm{mod},i} - v_{\mathrm{obs},i})^2} \quad (1)$$

$$\mathrm{rRMSE} = \frac{\mathrm{RMSE}}{\bar{v}_{\mathrm{obs}}} \quad (2)$$

The mean bias error (MBE) is used to assess the overall bias of the modeled wind compared to the observational wind speeds. It is taken as the average difference between the modeled wind speeds and the observed wind speeds. Values can be negative or positive and indicate any systematic biases present within the model. For example, a negative bias would indicate that the model systematically underestimates wind speeds and vice versa. Zero indicates either the model performs realistically or there is equal amount of positive and negative biases. In Eq. (3) below $\boldsymbol{v_{mod}}$ represents the modeled wind speeds and $\boldsymbol{v_{obs}}$ represents the observed wind speeds. Relative MBE (rMBE) was also considered, Eq. (4), by dividing the MBE by the average

Table 2. Information for the hub-height wind data sourced from meteorological towers across CONUS. The number listed for each location corresponds to the numbers in Fig. 1, identifying the geographic positions of the meteorological towers. Location coordinates for proprietary data were excluded.

Geography	Location	Coordinates	Temporal Coverage	Anemometer Height
W. Coast	Megler, WA (1)	46.27°N, -123.88°W	2010-2018	53m
	Martinez, CA (3)	38.04°N, -122.12°W	2014-2020	100m
	Los Angeles Pier J, CA (4)	33.73°N, -118.19°W	2014-2020	31m
Mountain	Wasco, OR (2)	45.50°N, -120.77°W	2005-2018	30m
	NWTC, CO (5)	39.91°N, -105.24°W	2002-2020	50m
Plains	Site A, KS (6)	-	2006-2008	49m
	SGP Observatory, OK (7)	36.61°N, -97.49°W	2012-2020	65m
	Site A, TX (8)	-	2008-2013	50m
	Site B, TX (9)	-	2009-2013	51m
	Site A, MN (10)	-	2007-2011	80m
	Site A, AR (11)	-	2011-2012	53m
	Argonne National Lab, IL (12)	41.70°N, -87.99°W	2007-2013	60m
	Site A, IN (13)	-	2018-2019	90m
	Site A, OH (14)	-	2017-2018	90m
Great Lakes	Dunkirk, NY (17)	42.49°N, -79.35°W	2001-2017	20m
E. Coast	Edith Hammock, AL (15)	30.23°N, -88.02°W	2008-2013	36m
	Fowey Rock, FL (16)	25.59°N, -80.09°W	2001-2020	44m
	Spiderweb, SC (18)	33.41°N, -81.83°W	2009-2012	34m
	East Point, FL (19)	29.41°N, -84.86, °W	2004-2020	35m
	Cape Henry, VA (20)	36.93°N, -76.01°W	2007-2020	28m
	Brookhaven, NY (21)	40.87°N, -72.89°W	2007-2013	50m
Alaska	Red Dog Dock, AK (22)	67.58°N, -164.07°W	2018-2020	13m
	Bligh Reef, AK (23)	60.84°N, -146.88°W	2013-2020	22m
	Juneau Dock, AK (24)	58.29°N, -134.39°W	2018-2020	18m
	Five Fingers, AK (25)	57.27°N, -133.63°W	2013-2020	22m
Puerto Rico	San Juan, PR (26)	18.43°N, -66.01°W	2001-2020	10m

of the observed wind speed. This gives a general sense of the magnitude of bias in relation to the magnitude of the wind speeds themselves.

$$MBE = \frac{1}{n}\sum_{i=1}^{n}(v_{mod,i} - v_{obs,i}) \tag{3}$$

$$rMBE = \frac{MBE}{\bar{v}_{obs}} \tag{4}$$

The Pearson correlation coefficient (r) measures the degree of linear correlation in time between model wind speeds and observational wind speeds. Values range from -1 to 1, with -1 indicating a perfect negative correlation, 1 indicating a perfect positive correlation, and 0 indicating no correlation. In Eq. (4) below, $\boldsymbol{\bar{v}_{\mathrm{mod}}}$ is the mean of the modeled wind speeds and $\boldsymbol{\bar{v}_{\mathrm{obs}}}$ is the mean of the observed wind speeds.

$$r = \frac{\sum_{i=1}^{n}(v_{\mathrm{mod},i}-\bar{v}_{\mathrm{mod}})(v_{\mathrm{obs},i}-\bar{v}_{\mathrm{obs}})}{\sqrt{\sum_{i=1}^{n}(v_{\mathrm{mod},i}-\bar{v}_{\mathrm{mod}})^2 \sum_{i=1}^{n}(v_{\mathrm{obs},i}-\bar{v}_{\mathrm{obs}})^2}} \tag{5}$$

Lastly, overlap coefficients (OVLs) were calculated between the probability density functions for the modeled and observed wind speed distributions, using Eq. (5). Functions were estimated using kernel density estimations, specifying Scott's rule (Scott, 2015) for bandwidth smoothing. Once functions were drawn, OVLs were calculated using the following formula, in which $\boldsymbol{f_{v_{\mathrm{mod}}}(x)}$ is the estimated density function for the model wind speeds and $\boldsymbol{f_{v_{\mathrm{obs}}}(x)}$ is the estimated density function for the observed wind speeds. The result of this calculation yields a value from 0 to 1, in which 0 indicates no overlap and 1 denotes complete overlap between the estimated functions for observations and model wind speeds.

$$\mathrm{OVL} = \int_{-\infty}^{\infty}\left(f_{v_{\mathrm{mod}}}(x), f_{v_{\mathrm{obs}}}(x)\right)\,\mathrm{d}x \tag{6}$$

In addition to wind speed evaluations, we also conducted wind direction validations using wind roses. This is important for examining the model's performance in capturing the seasonality of wind direction, as well as for investigating the covariance of wind speed and direction (Wu et al., 2022b). For these wind roses, similarity indices (WRSIs) were also calculated by taking the sum of the minimum frequencies between model and observations for each discrete wind direction bin, using Eq. (6). Here, $\boldsymbol{f_{d_{\mathrm{mod}}}(i)}$ and $\boldsymbol{f_{d_{\mathrm{obs}}}(i)}$ represent the frequency of wind directions for each bin i.

$$\mathrm{WRSI} = \sum_{i}^{n}\min(f_{d_{\mathrm{mod}}}(i), f_{d_{\mathrm{obs}}}(i)) \tag{7}$$

2.5 Uncertainty Quantification

To quantify model uncertainty due to internal variability and structure uncertainty as described in Section 2.2, statistical bootstrapping was employed on the sixteen 1-year simulations to generate 500 augmented ensemble members. This was done by randomly selecting data for each hour from one of the sixteen ensembles, ultimately building an entirely new ensemble with the same spatial and temporal domain. This technique allows for a more comprehensive look at the statistical distribution of data and the underlying variability that drives model uncertainty. Time averages were then performed across the model domain on each of the 500 resampled ensembles to gauge how the degree of model uncertainty is influenced by different timescales; this included monthly, bi-weekly, weekly, and daily averages, as well as daytime (21 UTC) and nighttime (06 UTC) monthly averages. To represent model uncertainty, 5^{th} and 95^{th} percentiles were taken at the different time scale averages (e.g., weekly and biweekly) across the 500 augmented ensembles to determine the upper and lower bounds of temporally averaged wind speeds. Then, the difference between these two percentiles (95th - 5th) served to demonstrate the degree of ensemble spread. These percentiles were calculated for every grid point and at each timescale average to reveal spatiotemporal patterns present for model uncertainty. Interannual variability was calculated as well to compare with model uncertainty. The same timescale averages were taken before computing the same percentiles (5^{th} and 95^{th}) across the 20-year period.

3 Results

3.1 Hub-Height Wind speed and Wind Direction Validations

We start with a model validation for wind speeds at hub-heights (Section 2.2) over the 26 locations (Fig. 1) to assess ADDA-v2's utility for wind energy applications. We used several metrics and statistics to quantify model performance, including probability density functions (PDFs), mean biases, seasonally averaged wind speed diurnal cycles, wind roses, time-scale dependent RMSEs and correlation coefficients. For each figure, locations from the different geographies listed in Table 2 were chosen to assess ADDA-v2's performance in different regions; where possible, at least one figure representing each geographic characteristic was displayed.

3.1.1 Probability Density Functions

PDFs effectively compare data distributions without considering the time dimension, aiming to visualize any biases between model and observation. Across the 26 hub-height locations, ADDA-v2's PDFs had a higher average OVL of 0.85 with the observational PDFs, while ERA5's PDFs had an average OVL of 0.78. Similarities between ADDA-v2 and ERA5 distributions and observed wind speeds were spatially variable, with ADDA-v2 performing better than ERA5 for 18 of the 26 sites considered. In particular, ADDA-v2's higher resolution was able to capture the finer scale wind speed patterns in mountainous regions, with OVLs significantly higher than ERA5's over the Cascades and the Rockies (Fig. 2c, d). ADDA-v2 was able to modestly outperform ERA5 across the Plains region. The average OVLs for ADDA-v2 across the nine locations was 0.86, while ERA5 saw an average OVL of 0.79. There were a couple locations where both datasets struggled to capture the hub-height wind speed distribution. For example, both ADDA-v2 and ERA5 demonstrated strong overestimations (Fig. 2j) for Spiderweb, South Carolina. As will be discussed in Section 3.3, ADDA-v2's positive bias can be partly attributed to the land surface model (LSM) used for these simulations, as well as the positive bias inherited by ERA5. Both datasets also struggled with the hub-height wind speeds at Brookhaven, New York. However, the overestimations seen for this location by both datasets may be attributed to its unique geographic position; it is located on Long Island, New York, equidistant from Long Island Sound and the Atlantic Ocean, where land sea interactions on either side may incite complexities in the local wind patterns. Across the four Alaska locations, ADDA-v2 saw an overage OVL of 0.88 compared to ERA5's 0.70 (Fig. 2k). ERA5's coarser resolution can contribute to these errors, especially across Alaska, where complex topography incites stark spatial changes in wind patterns. For San Juan, Puerto Rico, ADDA-v2 and ERA5 saw decent performance in capturing wind speed patterns, although both depicting modest overestimations (Fig. 2l).

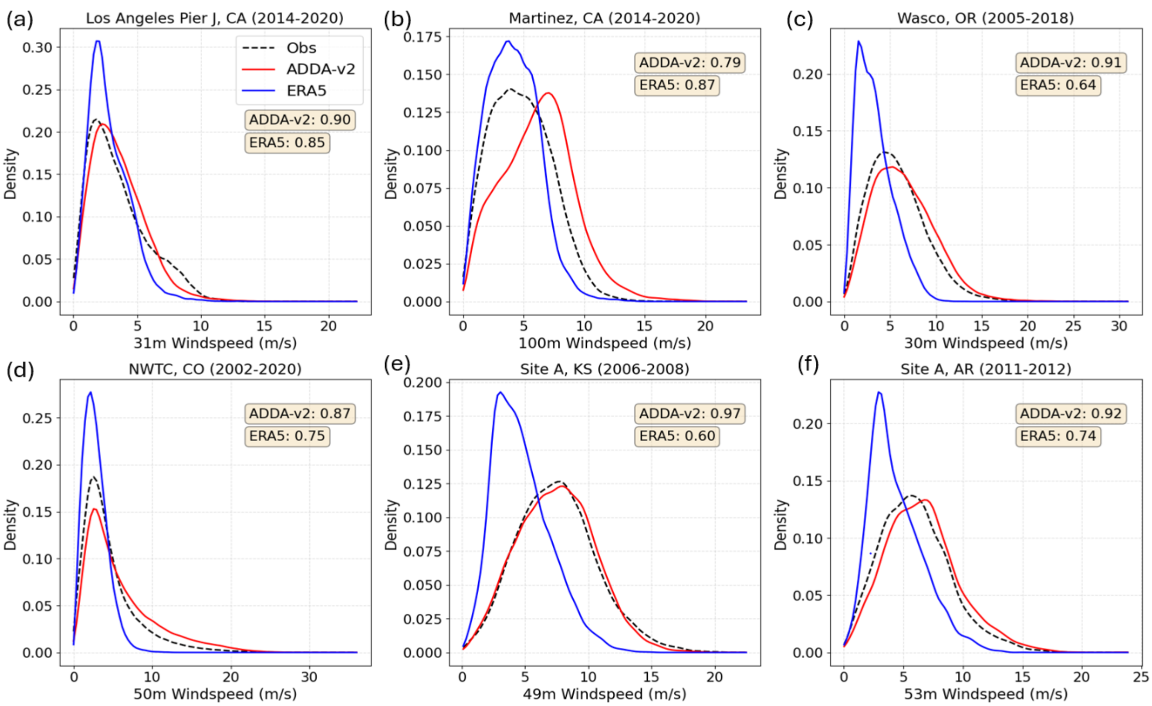

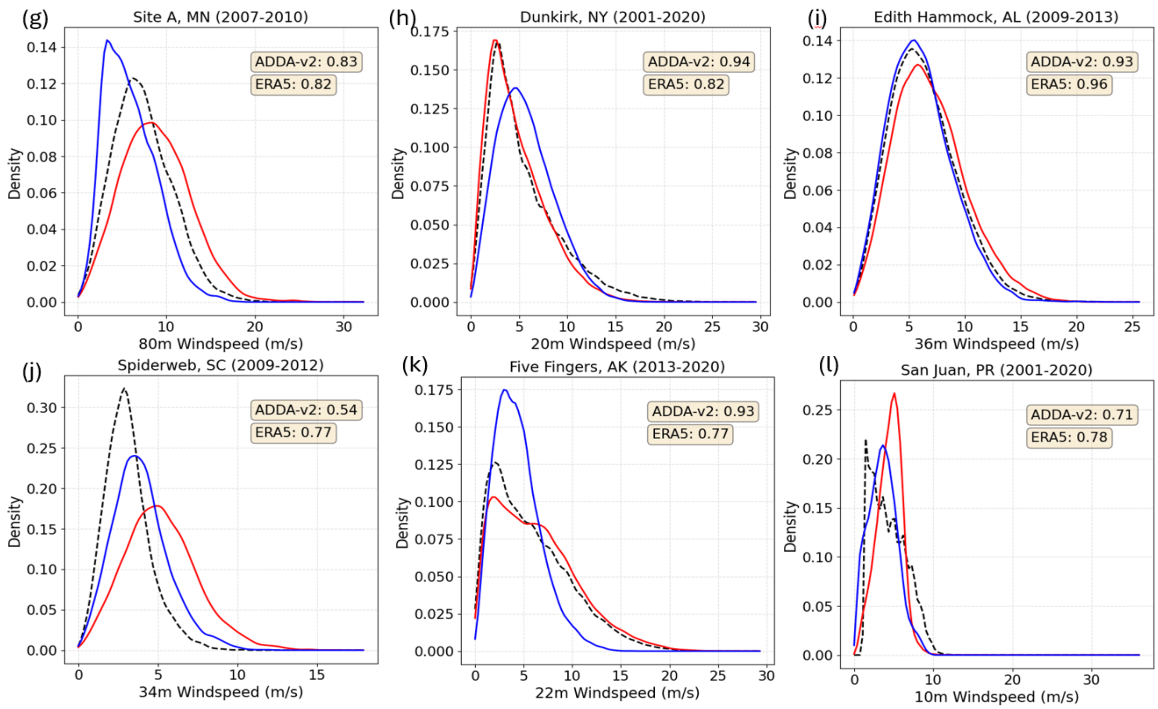

Figure 2. Probability density functions (PDFs) of ADDA-v2 and ERA5 simulated wind speeds alongside observations over Los Angeles Pier J, California (a), Martinez, California (b), Wasco, Oregon (c), NWTC, Colorado (d), Site A, Kansas (e), Site A, Arkansas (f) Site A, Minnesota (g), Dunkirk, New York (h), Edith Hammock, Alabama (i), Spiderweb, South Carolina (j), Five Fingers, Alaska (k), and San Juan, Puerto Rico.

3.1.2 Mean Bias

While PDFs provide a general view of model's systematic bias, they do not evaluate the time dimension. Mean bias is therefore examined here to identify any systematic errors present within our models when considering the time dimension. Here, the entire overlapping time periods between ADDA-v2, ERA5, and the observations were taken. At each daily-averaged (Table 3), monthly-averaged, and seasonally averaged timestep, the bias was taken between each dataset and observations. The interquartile range and the minimums/maximums of these bias values were then plotted in Fig. 3.

Across most of the locations, ADDA-v2's median biases are either centralized around 0 or slightly larger than zero, indicating that ADDA-v2 performs reasonably well with slight overestimations. However, ERA5 demonstrated clear underestimations across the locations sampled. For example, for the mountainous location Wasco, Oregon, ERA5 saw a strong negative MBE (Fig. 3a). Similarly for the Great Plains location, Site A, Kansas, ERA5 saw an equally large negative MBE of -2.79 m s^{-1}. ADDA-v2 had smaller MBEs for both locations at 0.67 m s^{-1} and -0.07 m s^{-1}, respectively. The East Coast and Caribbean locations, Fowey Rock, FL and San Juan, Puerto Rico saw minimal MBEs of 0.32 m s^{-1} and 0.02 m s^{-1} for ADDA-v2, and -1.66 m s^{-1} and -0.79 m s^{-1} for ERA5 (Fig. 3a). For Five Fingers, Alaska, MBE ranges were large for both ADDA-v2 and ERA5 at the daily timescale. ADDA-v2 outperformed ERA5 for this location, demonstrating a small positive bias compared to ERA5's modest underestimation. Lastly, both datasets had minimal MBEs for Los Angeles Pier J, California, with relatively small IQRs (Fig 3a).

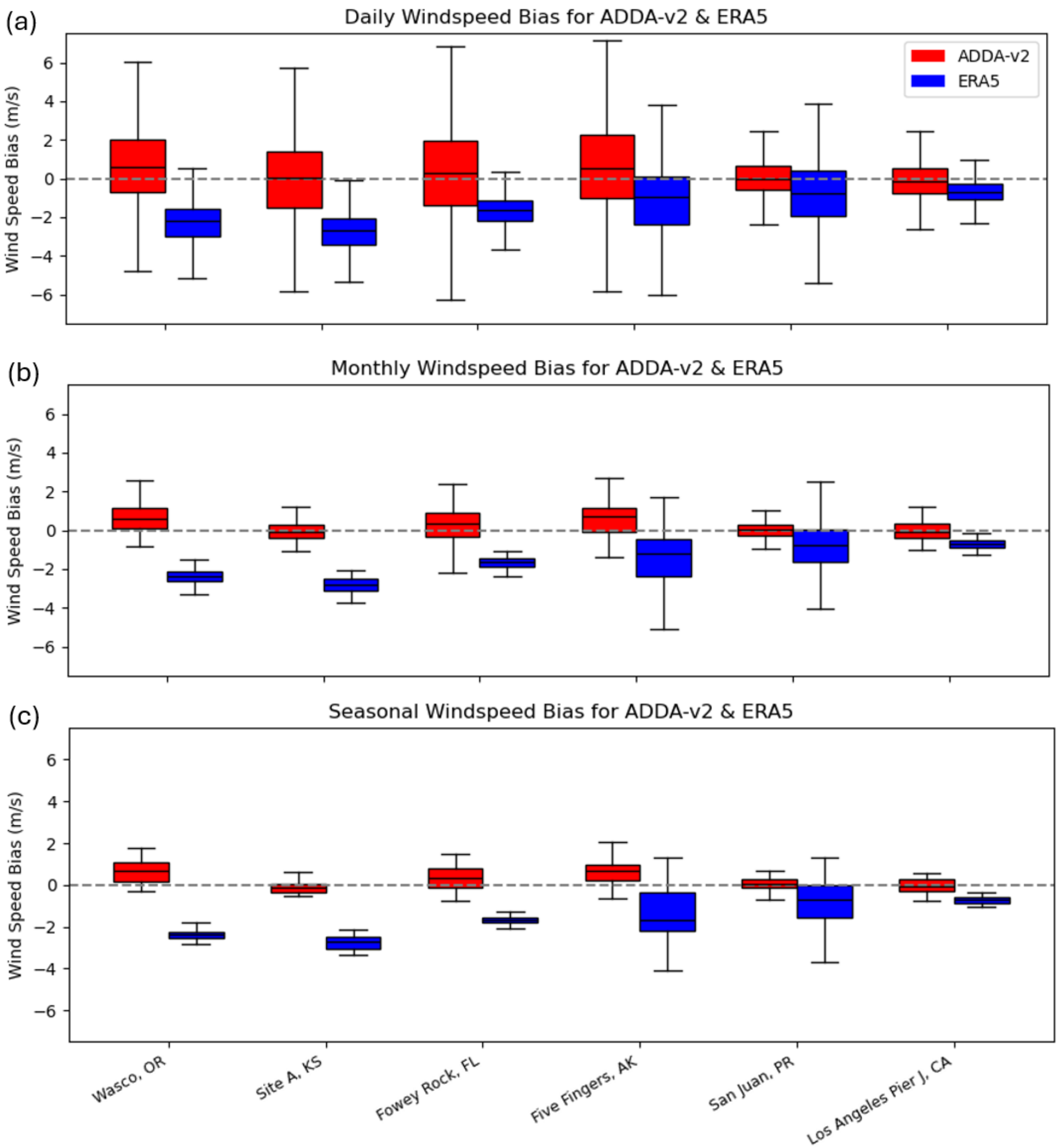

Figure 3. Distribution of mean biases computed between ADDA-v2 (red) and observations and between ERA5 and observations (blue) during the overlapping time periods, plotted as box-and-whiskers for Wasco, Oregon, Site A, Kansas, Fowey Rock, Florida, Five Fingers, Alaska, San Juan, Puerto Rico, and Los Angeles Pier J, California at the daily (a), monthly (b), and seasonal (c) timescales.

3.1.3 Diurnal Cycles

While PDFs and mean biases are useful in understanding the overall distribution and temporal accuracy of model simulated wind speeds, it is particularly crucial to understand how well the model captures diurnal variability of wind, especially when planning hybrid renewable energy assessments between wind and solar energies. Therefore, seasonally averaged wind speed diurnal cycles are considered in this analysis for each hub-height location to evaluate how well ADDA-v2 captures intraday wind speed patterns. Specifically, an average was taken for each hour of the day (00, 01, 02, etc.) across each season. Ten-meter wind speeds were also included for some of these locations because they have more pronounced diurnal patterns. Pearson's *r* and RMSE values are used to validate the seasonally averaged model diurnal cycles.

Across all locations (Fig. 1), ADDA-v2's diurnal wind speed patterns had an average Pearson's *r* of 0.67 with observations, while ERA5's average was considerably lower, at approximately $r = 0.35$. Similarly, ADDA-v2 had a lower average RMSE of 1.02 m s^{-1} compared to the 1.36 m s^{-1} RMSE of ERA5. Both datasets saw improved performance when there was a strong diurnal signature in wind speed magnitudes, as summarized in Table 3. This was especially the case for southern locations, especially with coastal geographies, where the greater surface heating at lower latitudes modulates diurnal wind speed patterns more significantly (Elliott et al. 2004). For East Coast locations like East Point, Florida, Fowey Rock, Florida, and Edith Hammock, Alabama, Pearson's *r* were at or above 0.85 for ADDA-v2. ERA5 Pearson's *r* were also high overall, but the dataset struggled with Fowey Rock in particular (Fig. 4b). Overall, ADDA-v2 performed better for the wind speed diurnal pattern for the West Coast region (Fig. 4a) with an average Pearson's *r* of 0.74 compared to ERA5's 0.64. However, ADDA-v2 did tend to overestimate wind speeds for Martinez, California and Wasco, Oregon, leading to higher RMSE values compared to ERA5. For regions with flat terrain, ADDA-v2 performed much better than ERA5. Correlation coefficients for plain-like geographies, on average, were $r = 0.76$ for ADDA-v2 and $r = 0.27$ for ERA5. For mountainous regions, both ADDA-v2 and ERA5 struggled significantly to capture diurnal wind speed patterns (Fig. 4c), with an average Pearson's *r* of 0.32 and 0.24 respectively. The high elevations of these locations have more complex responses to diurnal changes in solar heating and thus do not have very clear wind speed patterns throughout the day, especially during the winter (Fig. 4c). Across the four Alaska locations, both datasets struggled to capture the diurnal pattern, with an average Pearson's *r* of 0.46 for ADDA-v2 and 0.12 for ERA5. Lastly, for San Juan, Puerto Rico, both datasets were able to capture the dramatic diurnal wind speed pattern observed (Fig. 4e). However, ADDA-v2 was much more precis accurately simulating intraday wind speed minimums and maximums.

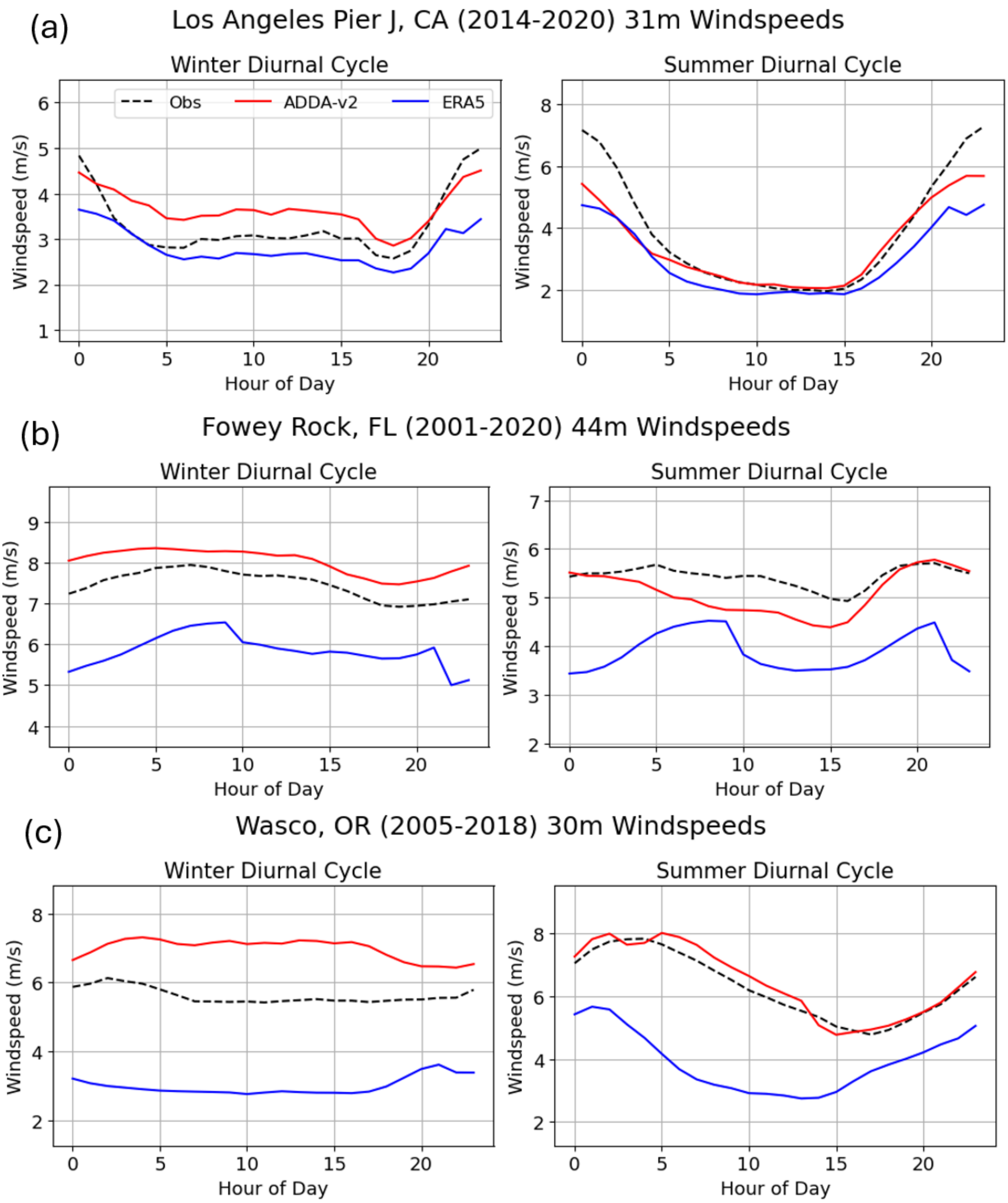
(a)
Los Angeles Pier J, CA (2014-2020) 31m Windspeeds
Winter Diurnal Cycle
Summer Diurnal Cycle
Obs
ADDA-v2
ERA5
Windspeed (m/s)
Hour of Day
(b)
Fowey Rock, FL (2001-2020) 44m Windspeeds
Winter Diurnal Cycle
Summer Diurnal Cycle
Windspeed (m/s)
Hour of Day
(c)
Wasco, OR (2005-2018) 30m Windspeeds
Winter Diurnal Cycle
Summer Diurnal Cycle
Windspeed (m/s)
Hour of Day

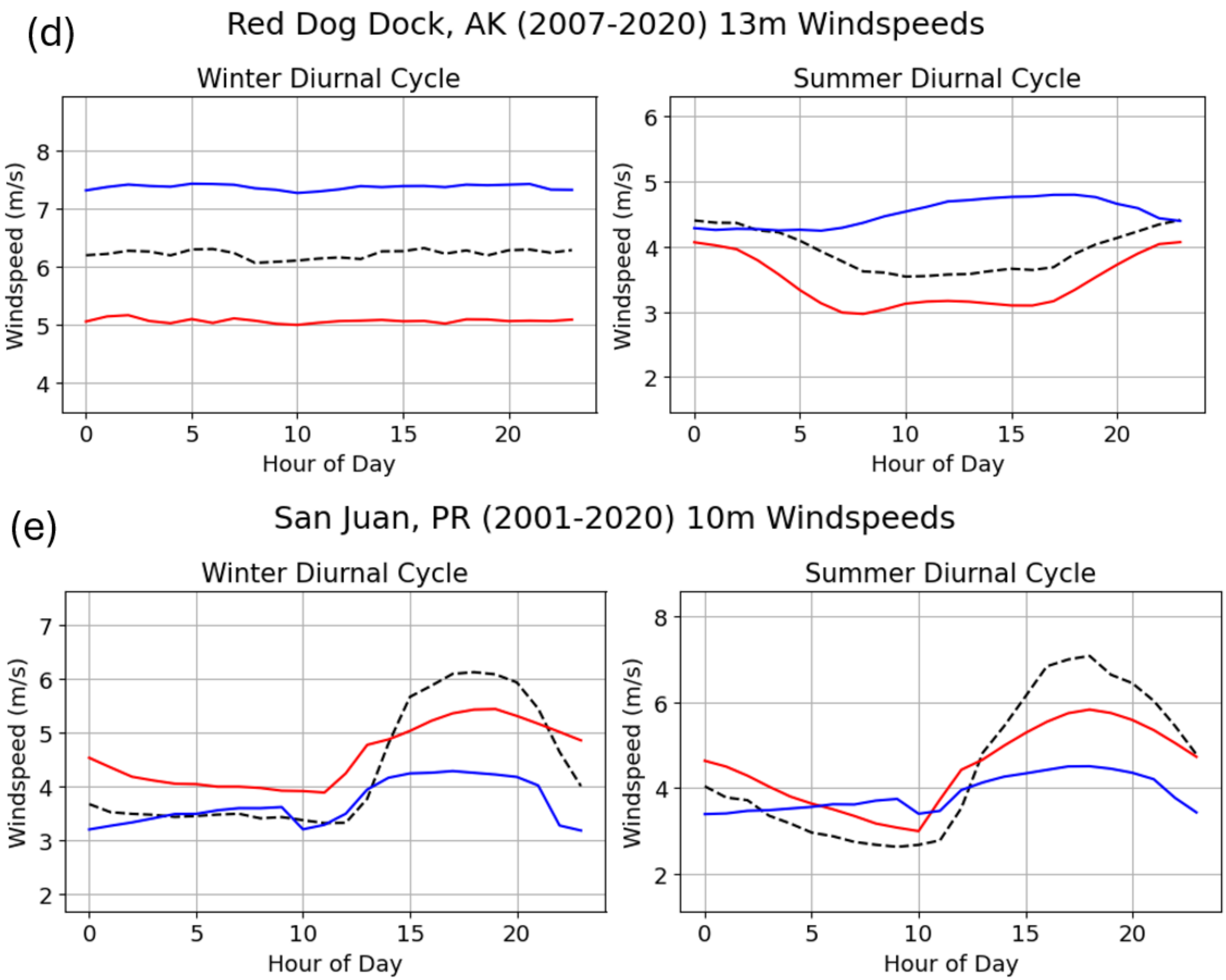

Figure 4. Seasonally averaged diurnal wind speeds (summer, winter) for Los Angeles Pier J, California (a), Fowey Rock, Florida (b), Wasco, Oregon (c), Red Dog Dock, Alaska (d), and San Juan, Puerto Rico (e).

3.1.4 Wind Roses

Previous sections focus on assessing model performance for wind speeds, but it is also important to assess model performance for wind direction to indicate whether the model can capture synoptic scale phenomena that drive these seasonal changes in wind direction. Wind direction is also important for understanding the wake effect in a large wind farm. This section employs wind roses to visualize seasonal wind direction distributions for each hub-height location between model and observations.

Across the 19 locations that had available wind direction data, both ADDA-v2 and ERA5 were able to reasonably capture the climatological synoptic mechanisms driving seasonal changes in wind directions, with WRSI at 0.75 and 0.74 respectively. No single geographic region within ADDA-v2 significantly outperformed another, as summarized in Table 3.

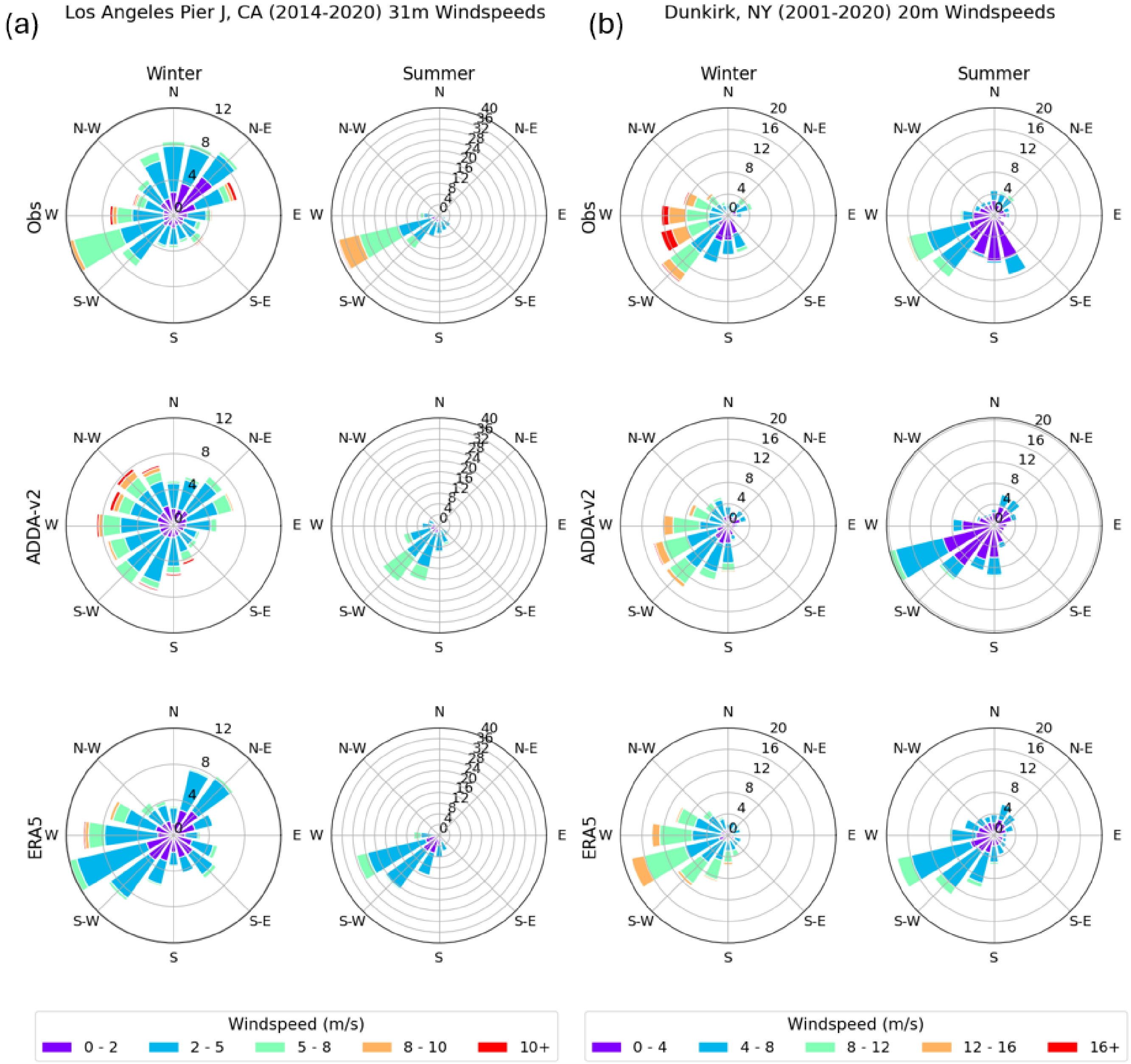
(a)
Los Angeles Pier J, CA (2014-2020) 31m Windspeeds
(b)
Dunkirk, NY (2001-2020) 20m Windspeeds
Winter
Summer
Obs
ADDA-v2
ERA5
N
N-E
E
S-E
S
S-W
W
N-W
Windspeed (m/s)
0 - 2
2 - 5
5 - 8
8 - 10
10+
0 - 4
4 - 8
8 - 12
12 - 16
16+

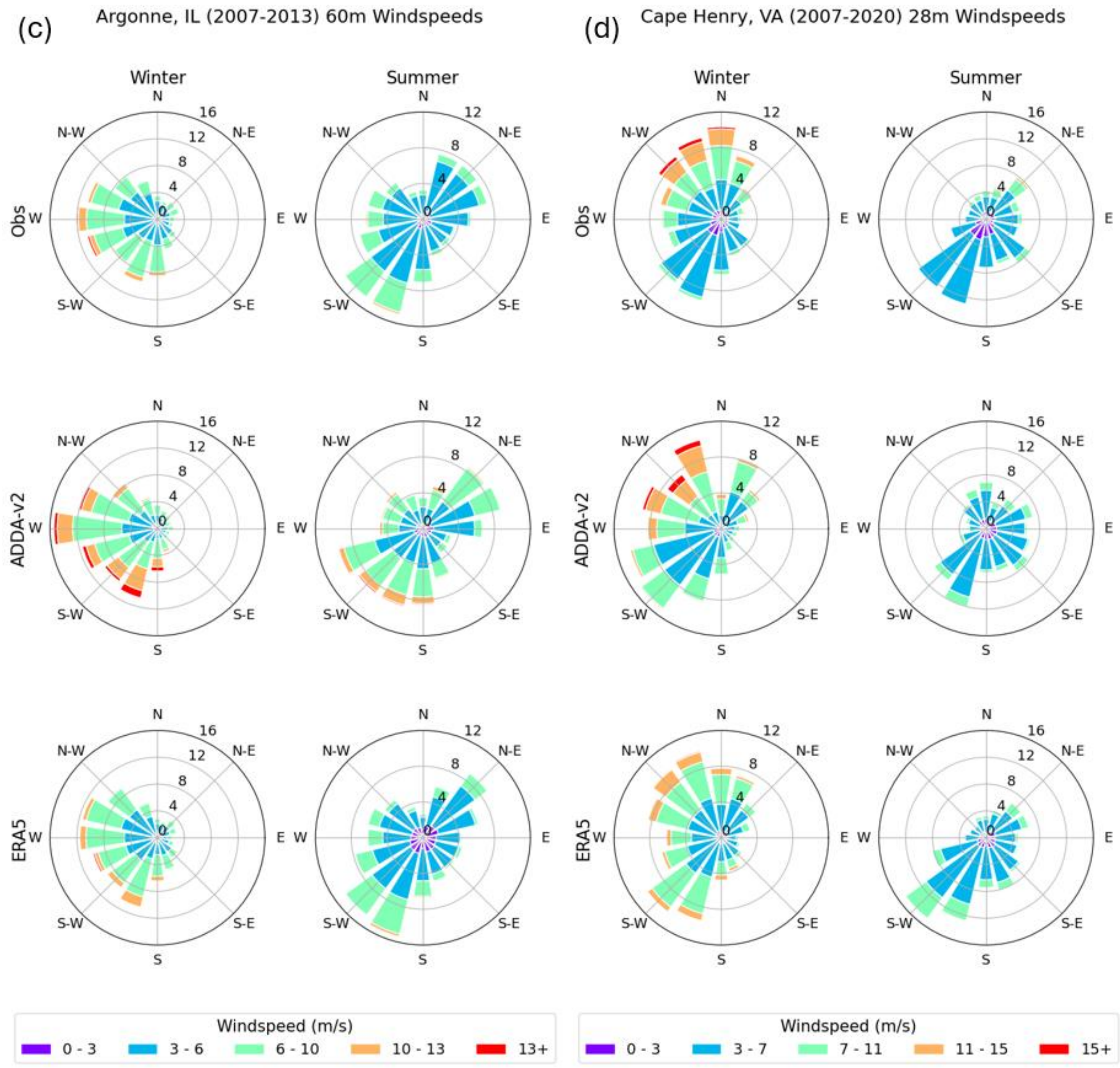

Figure 5. Seasonally averaged wind speed and wind direction distributions for Los Angeles, Pier J, California (a), Dunkirk, New York (b), Argonne, Illinois (c), and Cape Henry, Virginia (d). Values on each concentric circle (e.g., 4, 8, 12, 16) within the wind rose are used to measure the normalized frequency of each wind direction wedge. Windrose wedge positions indicate the direction from which the wind is blowing.

However, ADDA-v2 outperformed ERA5 for the mountainous location, NWTC, Colorado, with WRSIs of 0.90 and 0.69, respectively. Here, ADDA-v2 was able to accurately capture the predominantly west winds in the fall, winter, and spring, generated by mid-latitude cyclones and the more mesoscale chinook winds that occur on the leeward sides of mountain ranges (Lackman, 2011; Markowsi & Richardson, 2010). Diurnal patterns of wind direction were also evaluated (Fig. S1). While both ADDA-v2 and ERA5 captured the intraday wind direction patterns of these locations examined, ADDA-v2 is able to more correctly simulate the wind direction shift ERA5 in the afternoon during the summer when wind direction has more abrupt changes due to diurnal heating and cooling.

Across the Alaska locations, ADDA-v2 performed moderately well, with wind direction WRSIs at Bligh Reef, Five Fingers, Juneau Dock, and Red Dog Dock (Fig. 5d) at 0.72, 0.81, 0.79, and 0.66. For coastal locations, like Red Dock, Alaska, summer wind directions can be influenced by sea breezes, indicated by the high frequency of southerly flow during the summer (Fig. 5d).

3.1.5 Model Performance Across Various Time Scales

The model setup for ADDA-v2 is designed for capturing climatological statistics rather than predicting day-to-day weather (Appendix A in Wang et al., 2014). However, it can still be used to understand average intraday wind speed patterns for different regions. This section tests ADDA-v2's capacity to represent wind speeds at different timescales using RMSEs and correlations, aiming to demonstrate the timescale in which the model can be useful for wind energy resource assessments.

For almost all hub-height locations analyzed, RMSEs decreased, and correlations increased as the time scale averages became coarser. On average across the 26 locations considered, rRMSEs at the daily, weekly, biweekly, and monthly scale were 46%, 29%, 25%, and 22% respectively, indicating improvement at each transition to a coarser timescale (Fig. 6f). Pearson's r showed a similar trend, at $r = 0.48$, $r = 0.63$, $r = 0.68$, and $r = 0.75$ (Fig. 6f), consistently growing when calculated at increasingly coarse timescales. Also, the largest error improvement occurred when going from daily averages to weekly averages. For example, this can be seen for the 60m wind speeds at Site A, Arkansas (Fig. 6b), where rRMSEs were at 37% at the daily timescale, before dropping to 20%, 16%, and 13% at the weekly, biweekly, and monthly timescales. Pearson's r also improved from 0.57 at the daily time scale to 0.89 at the monthly time scale. Similarly, Fowey Rock, FL (Fig. 6b) sees a drastic improvement from daily to weekly averaged wind speeds, with rRMSEs dropping from 40% to 23%, and Pearson's r steadily climbing between timescale averages. This trend is seen for the Alaska and Puerto Rico locations as well, with ADDA-v2 struggling to capture specific-day wind speeds, but performing well at coarser, more climatological time scales (Fig. 6c, d)

Table 3 Statistical metrics for each of the 26 hub-height observational locations.

Geography	Location	Wind speed OVL		Wind speed Diurnal Correlation		Wind speed Diurnal RMSE (m s^{-1})		WRSI		Wind speed MBE (m s^{-1})	
		ADDA-v2	*ERA5*	*ADDA-v2*	*ERA5*	*ADDA-v2*	*ERA5*	*ADDA-v2*	*ERA5*	*ADDA-v2*	*ERA5*
W. Coast	Megler, WA	0.82	0.94	0.85	0.35	1.45	0.40	0.68	0.73	1.44	-0.15
	Martinez, CA	0.79	0.87	0.39	0.64	1.64	0.86	0.61	-	1.38	-0.66
	Los Angeles Pier J, CA	0.90	0.85	0.97	0.94	0.64	0.90	0.69	0.72	-0.02	-0.70
	Average	**0.84**	**0.89**	**0.74**	**0.64**	**1.24**	**0.72**	**0.66**	**0.73**	**0.93**	**-0.50**
Mountain	Wasco, OR	0.91	0.64	0.69	0.4	0.78	2.53	0.63	0.65	0.67	-0.07
	NWTC, CO	0.87	0.75	-0.05	0.07	1.64	1.86	0.90	0.69	1.65	-1.78
	Average	**0.89**	**0.69**	**0.32**	**0.24**	**1.21**	**2.2**	**0.77**	**0.67**	**1.08**	**-0.78**
Plains	Site A, KS	0.97	0.6	0.89	0.03	0.40	2.88	-	-	-0.07	-2.79
	SGP Observator y, OK	0.90	0.89	0.83	0.89	0.52	0.76	0.79	0.77	0.85	-0.96
	Site A, TX	0.83	0.63	0.91	-0.30	1.18	3.14	-	-	-1.12	-2.99
	Site B, TX	0.97	0.8	0.75	0.89	0.46	1.37	-	-	0.07	-1.28
	Site A, MN	0.83	0.82	0.90	-0.38	1.62	1.59	0.83	-	1.46	-1.39
	Site A, AR	0.92	0.74	0.48	0.40	0.72	1.66	-	-	0.58	-1.62
	Argonne, IL	0.76	0.89	0.64	0.55	1.15	0.35	0.82	0.81	1.12	-0.07
	Site A, IN	0.76	0.93	0.59	0.41	1.66	0.60	0.68	-	1.39	0
	Site A, OH	0.82	0.81	0.82	-0.08	1.40	1.33	0.78	-	1.33	-1.07
	Average	**0.86**	**0.79**	**0.76**	**0.27**	**1.01**	**1.52**	**0.78**	**0.79**	**0.62**	**-1.35**
Great Lakes	Dunkirk, NY	0.93	0.82	0.82	-0.33	0.67	0.63	0.83	0.81	-0.65	0.36
E. Coast	Edith Hammock, AL	0.93	0.96	0.86	0.93	0.59	0.31	0.72	0.76	0.57	-0.27

	Fowey Rock, FL	0.95	0.77	0.85	0.51	0.54	1.70	0.77	0.69	0.32	-1.66
	Spiderweb, SC	0.54	0.77	0.62	0.23	2.09	0.84	-	-	2.03	0.34
	East Point, FL	0.92	0.95	0.92	0.95	0.68	0.31	0.70	0.73	0.64	-0.26
	Cape Henry, VA	0.85	0.82	0.54	0.55	0.85	0.77	0.80	0.79	0.70	0.67
	Brookhaven, NY	0.63	0.56	0.51	0.49	2.36	2.88	-	-	2.18	2.51
	Average	**0.80**	**0.81**	**0.72**	**0.61**	**1.19**	**1.14**	**0.75**	**0.74**	**1.07**	**0.22**
Alaska	Red Dog Dock, AK	0.85	0.69	0.57	-0.11	0.70	1.20	0.66	-	-0.67	1.14
	Bligh Reef, AK	0.90	0.86	0.39	0.25	0.55	0.96	0.72	-	0.26	-0.79
	Juneau Dock, AK	0.83	0.47	0.48	0.33	0.90	2.90	0.79	-	-0.40	-2.86
	Five Fingers, AK	0.93	0.77	0.40	0.01	0.60	1.50	0.81	-	0.59	-1.33
	Average	**0.88**	**0.70**	**0.47**	**0.12**	**0.69**	**1.64**	**0.75**	**-**	**-0.06**	**-0.96**
Caribbean	San Juan, PR	0.71	0.78	0.95	0.62	0.62	1.15	0.88	-	0.02	-0.79
All	**Average**	**0.85**	**0.78**	**0.67**	**0.35**	**1.02**	**1.36**	**0.75**	**0.74**	**0.63**	**-0.80**

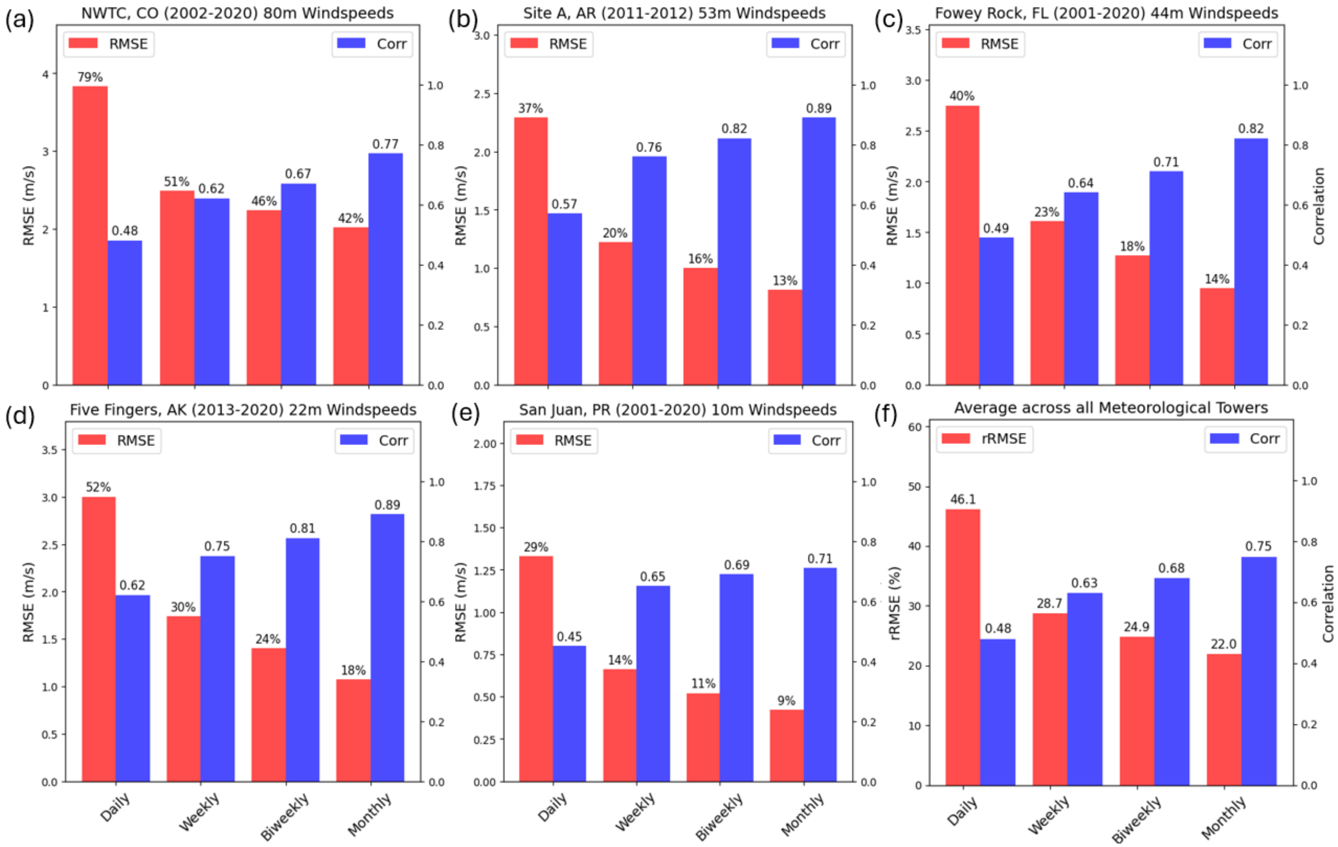

Figure 6. ADDA-v2 RMSEs, rRMSEs, and Pearson correlation coefficients at different timescale averages for Site A, Arkansas (b), Fowey Rock, Florida (c), San Juan, Five Fingers, Alaska (d), Puerto Rico (e), along with average metrics across all 26 meteorological towers (f). The number on each bar represents the value for each respective statistic, with time scales becoming coarser from left to right.

3.2 Near-surface Wind speed Evaluation

ADDA-v2 near-surface validations were initially performed using wind speed observations taken from 2,000+ ASOS stations across CONUS, Alaska, and Puerto Rico. While the full temporal domain (2001-2020) of ADDA-v2 was used in this analysis, statistics for each ASOS station were dependent on the maximum overlap in data availability between ADDA-v2 and observations. Seasonal means were taken across the available temporal period before calculating relative mean bias error (rMBE) and RMSE values for each ASOS station.

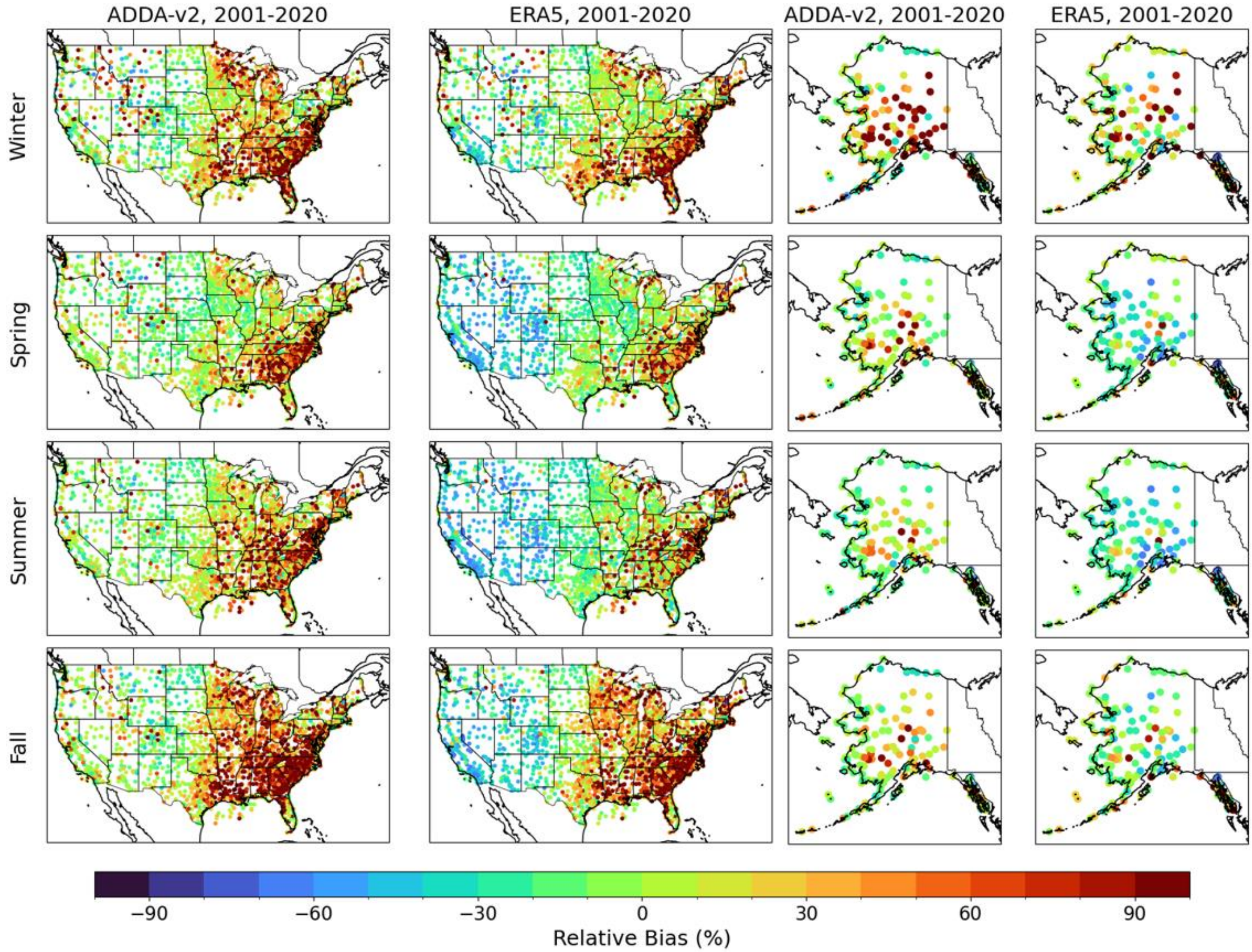

Figure 7. ADDA-v2 and ERA5 seasonal rMBEs calculated against 2,000+ ASOS locations across CONUS and Alaska.

ADDA-v2 performs well for the majority of ASOS stations evaluated, with rMBE values falling between -10-10% across much the western and central portions of the model domain. However, ERA5 struggles significantly in these same regions, especially in the spring and summer (rMBEs upwards of -60%). This has been documented in past studies (Chen et al., 2024; Wilczak et al., 2024), which highlight ERA5's tendency to underestimate wind speeds in areas of complex terrain (i.e., the Rockies).

For the eastern half of CONUS, both ADDA-v2 and ERA5 show similar spatiotemporal patterns for error magnitudes. Specifically, both datasets demonstrate notable rMBE values across the Southeast (60-80%), most notably during the fall and winter. This systematic error is predominantly attributed to model overestimation during nighttime hours (00-12 UTC), when observational wind speeds are very low (0-1 m s^{-1}), which is at a scale typical of model uncertainty. Thus, when the model simulates wind speeds of about 1.5-2 m/s, the relative error appears significant. Interestingly, ADDA-v2 also shows higher rMBE values for the upper Midwest during the fall and winter, when wind speeds are seasonally stronger; this bias is analyzed more in depth in Section 3.3. For most other regions, namely the central/lower Midwest, Texas, and the Northeast, ADDA-v2 and ERA5 accurately capture seasonal wind speeds, indicated by lower rMBE values.

When specifically looking at the ASOS stations over Alaska (Fig. 7), ADDA-v2 and ERA5 generally capture coastal wind speeds well with rMBEs around -15-15% but struggle more in areas with complex topography. For some locations of Alaska's mountainous interior, rMBE values are much higher than surrounding locations (rMBEs around 60%, especially during the winter). Overall, average RMSEs across Alaska for each season were 1.65, 1.08, 0.9, and 0.95 m s^{-1} for ADDA-v2 and 1.14, 1.23, 1.17, and 0.96 m s^{-1} for ERA5. Similarly to CONUS, ADDA-v2 was able to more accurately capture Alaska's wind speeds during the summer and fall but had a notable spike in RMSE magnitudes during the winter, especially for inland locations.

3.3 Sensitivity of Wind speed Biases to Physics Parameterizations

Given all the evaluations in previous sections, this section investigates some potential drivers of model bias over various regions which can be used to implement solutions. Most notably, ADDA-v2 sees positive wind speed biases across the Southeast United States, as well as for some parts of the Upper Midwest. This bias is seen for both the near-surface winds and the hub-height winds (Fig. 7, 2e). Part of these overestimations can be attributed to the biases within the forcing data ERA5. Depicted in Figure 7, ERA5 primarily overestimates wind speeds for southeast CONUS, especially during nighttime hours. Another potential reason for the overestimated wind speeds during night could be attributed to the model's capacity to respond to atmospheric stability. It has been documented that Noah-YSU (the PBL and LSM schemes used to run ADDA-v2 simulations) has an enhanced performance for wind speeds in unstable conditions but struggles in a very stable atmosphere (Hong et al. 2006, Draxl et al. 2014, Wang and Jin 2014). Thus, the very low wind speeds present during stable conditions may not be accurately captured by models employing these schemes.

The overestimation of wind speeds over the Upper Midwest, however, does not seem to be inherited from ERA5. Instead, it is likely due to the model's physics parameterization. Various ASOS locations were chosen in the Midwest where ADDA-v2 showed high error magnitudes to examine whether different physics parameterizations minimized these errors. Seasonally averaged diurnal cycles were studied for these locations using the six structure uncertainty ensemble members (Section 2.2) with varying PBL and LSM schemes against observations. Error metrics were calculated and the most accurate ensemble, indicated by the highest correlation coefficient or the lowest RMSE, was noted (Fig. 8).

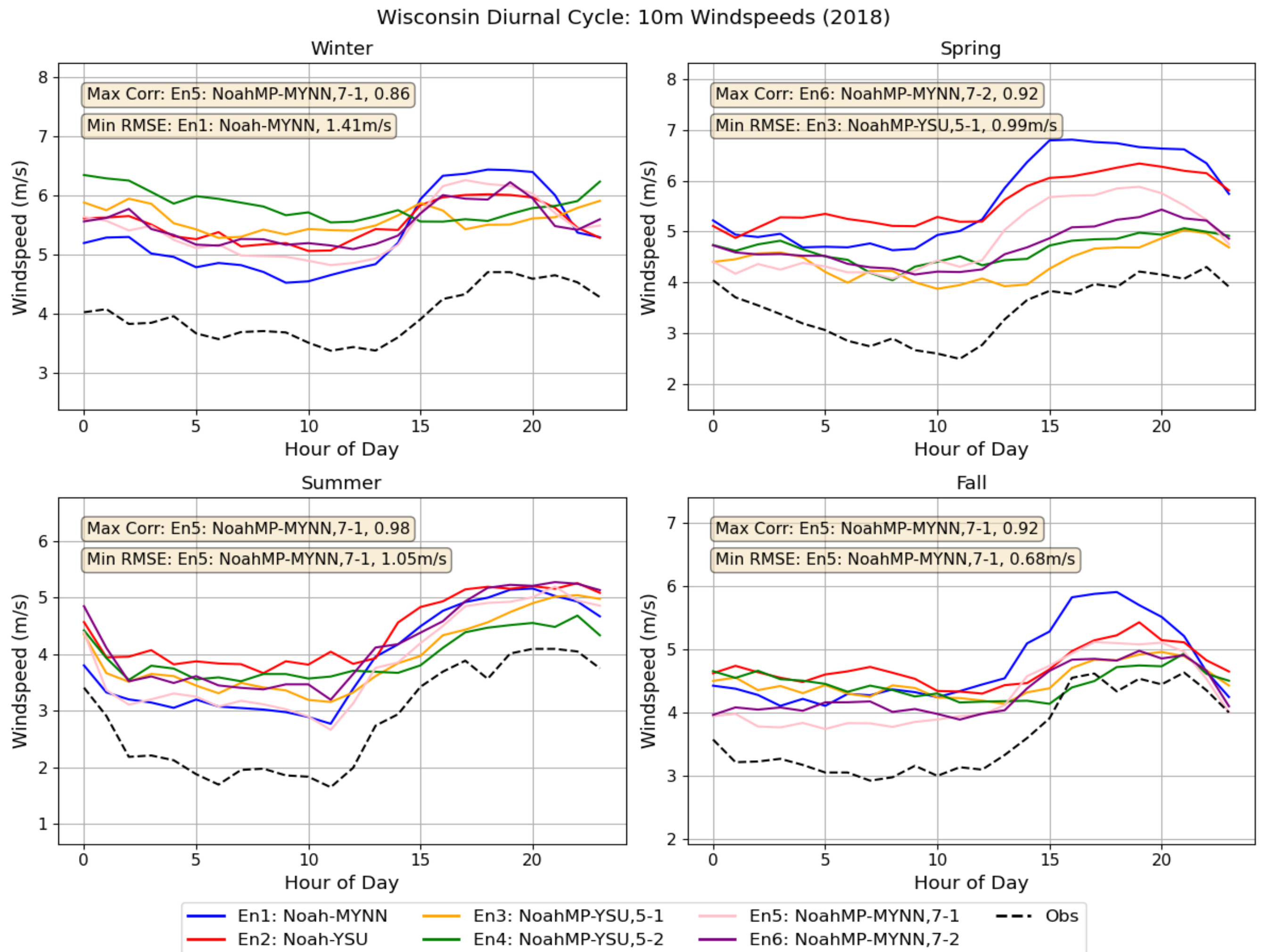

Figure 8. Seasonally averaged diurnal cycles for each of the structure uncertainty ensemble members (Section 2.4) against observed wind speeds in regions where ADDA-v2 demonstrated a positive bias. Each ensemble label is denoted by its LSM-PBL scheme, and the options for dynamic vegetation and surface layer drag coefficient calculation (e.g., 5-1 means dveg=5 and opt_sfc=1 in namelist.input if NoahMP was used).

For each location that demonstrated a positive near-surface wind speed bias, the Noah-MP land surface model outperformed the Noah land surface model, as seen in the diurnal cycles plotted for a Wisconsin ASOS station (Fig. 8). It is also apparent that the greatest error occurs during the overnight hours (00-12 UTC), in which none of the six ensemble members come close to representing the observed wind speeds. Contrarily, during the daytime hours (12-00 UTC), all ensemble members more accurately capture wind speed magnitudes, although still demonstrating some degree of overestimation. Furthermore, in all but one metric, the MYNN PBL scheme outperformed the YSU PBL scheme. Of the statistical metrics considered for each season, the MYNN PBL scheme almost always showed the lowest RMSE value and the highest correlation coefficient. However, it is important to acknowledge that no individual model configuration was able to solve the positive bias seen for these locations.

Considering the effects that different LSM schemes have on simulated wind speeds, we further analyzed how specific LSM parameterizations drive differences in near-surface winds. One of the most important considerations is the friction velocity, typically denoted by u_*. Friction velocity quantifies the turbulent momentum flux at the surface. Therefore, higher u_* values correspond to more of the momentum being lost to the surface, leading to weaker wind speeds closer to the ground.

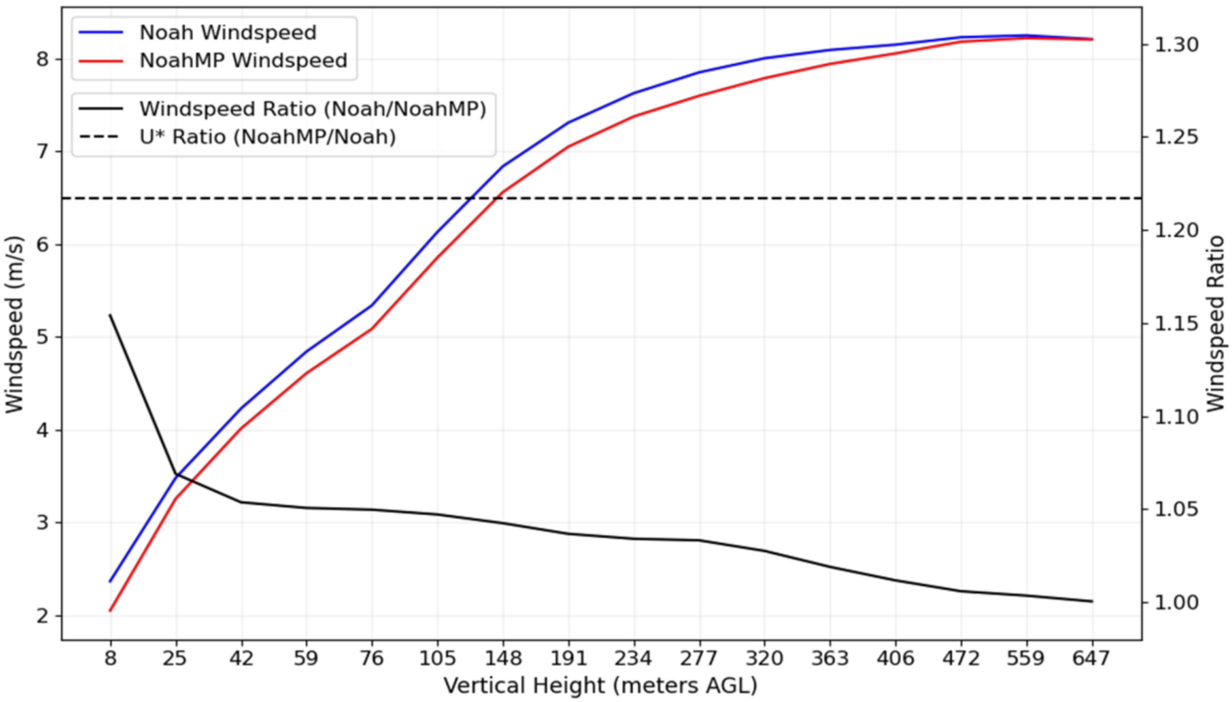

Figure 9. Vertical profile of wind for a location in which ADDA-v2 overestimated wind speeds, comparing averaged winds between the 2018 simulations using the NoahMP and Noah LSMs. Wind speed profiles correspond to the leftmost y-axis while the ratios of both wind speed and friction velocity use the rightmost y-axis.

We analyzed u_* between the Noah-MP and Noah LSM schemes and found that friction velocity generally tends to be larger in model simulations that employ Noah-MP (Fig. 9), especially at the locations that saw positive near-surface wind speed biases. In some cases, the friction velocity was as much as 20-25% larger in NoahMP than Noah. As a result, as shown in Fig. 9, wind speed ratios between NoahMP and Noah, specifically within the first ~10m AGL, were as high as 1.15 (Fig. 9). At greater heights (e.g., 25m and above), this ratio decreases as friction has a diminishing influence on momentum fluxes with increasing height as wind speeds get stronger overall. Therefore, while the NoahMP LSM saw improved performance in simulating near-surface winds, it still did not fully resolve the positive bias observed.

3.4 Interannual Variability and Model Uncertainty

Interannual variability across ADDA-v2's 20-year temporal period was calculated across the entire spatial domain. Additionally, model uncertainty was quantified by investigating the spread across 500 augmented ensembles, varying in their physics parameterizations (structure uncertainty) and initial conditions (internal variability). While the model uncertainty brought about by structure uncertainty was larger than that generated by the internal variability (Fig. S2), both were considered here to encompass a comprehensive look at all model uncertainty. The magnitudes and spatiotemporal patterns of each of these variabilities are then investigated here. Intuitively, the degree of model uncertainty is significantly influenced by the timescale being analyzed. This can be seen in Fig. 10, in which the magnitude of uncertainty scales inversely with the length of the timescale. The biweekly, weekly and daily timescales see overall uncertainty values of approximately 0.4-0.7 m s^{-1}, 0.7-1.1 m s^{-1} , and greater than 2.5 m/s, respectively, across much of North America (Fig.10, 11). This concept is similar to the improved performance of ADDA-v2 at coarser resolution timescales (Section 3.1.4). We also found that nighttime uncertainties were slightly higher than daytime uncertainties in regions of complex topography, especially over the Rocky Mountains.

In terms of spatial patterns of model uncertainty, the mountainous regions generally demonstrate higher uncertainty values, by about 0.5 m s^{-1}, when compared to adjacent regions with simpler topography (Fig. 10, Fig. 11a, b). This indicates that complex terrain introduces more unpredictable interactions between the physical mechanisms that drive near-surface and low-level wind (Wu et al., 2022a; Helbig et al., 2017). These interactions post challenges for the model to produce reasonable solutions. Thus, small changes in model initial conditions or parameterizations can influence these mechanisms and cause significant variability within the simulated wind. It is also interesting to note that large lake features also observed high degrees of model uncertainty, specifically during the summer months, indicating model's inadequacy of solving the air-lake interactions and the needs of a fully coupled lake-atmosphere model (Kayastha et al. 2023).

In the context of wind energy applications, model uncertainty is integral when mapping ideal locations for wind farm siting. However, it needs to be paired alongside spatiotemporal patterns of interannual variability to understand the full scope of wind resource reliability and potential risks associated with long-term power generation. Ideally, both model uncertainty and interannual variability need to be low for optimal and consistent power generation. As seen in Fig. 11a,b, the relative magnitude scale of interannual variability and model uncertainty is very different for all seasons. For example, the interannual variability of biweekly averaged 100 m wind speeds can be as high as 70-80% of the wind speed themselves. This is observed especially during the winter months, when highly variable synoptic-scale features strongly influence wind patterns. Alternatively, model uncertainty exists on a smaller magnitude, typically in the range of about 10-20% of the mean wind speed. The interannual variability in summer is smaller, with typical magnitudes ranging from 30-40% of the mean wind speed, likely attributed to the more consistent synoptic patterns present during summer. At coarser timescales (e.g. seasonal), both interannual variability and model uncertainty decrease considerably. Across much of North America, seasonal interannual

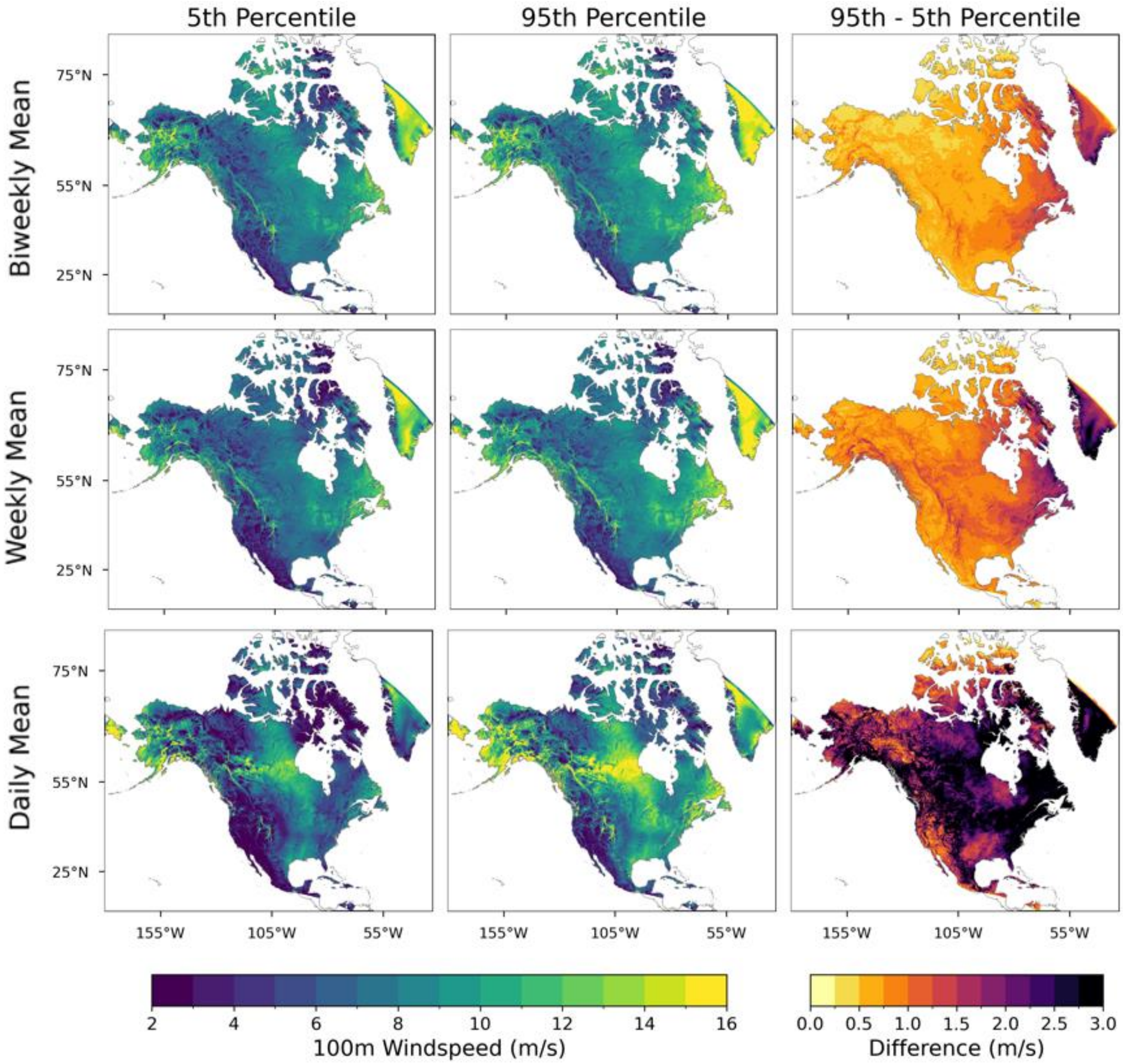

Figure 10. Model uncertainty at different timescale averages (daily, weekly and biweekly), represented by the difference between the 95th and 5th percentiles of the wind speed distributions.

variability is 15-25% of the mean wind speed. But, consistent with any timescale, these values can get as high 40-50% in regions of complex topography (Fig. S3).

The short-term ensemble simulations can be leveraged with the long-term simulations to identify key regions that have an optimal combination of moderately strong wind speeds and relatively low model uncertainty and interannual variability. Ultimately, this will maximize energy output potential for optimally sited wind farms.

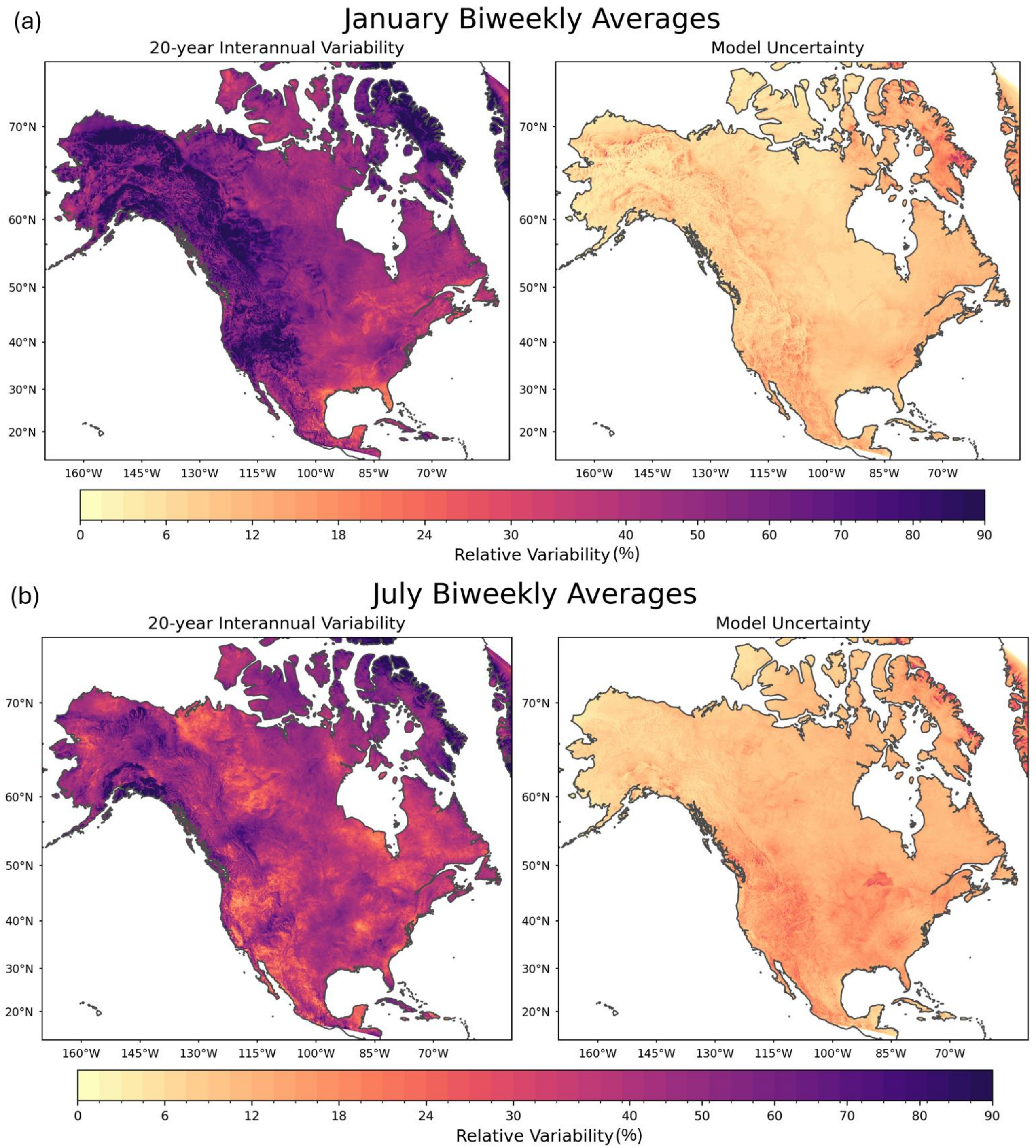

Figure 11. Relative interannual variability and relative model uncertainty for one biweekly averaged period for a winter month (January) and a summer month (July) for 100m wind speeds. Relative uncertainty and relative interannual variability were taken as the difference between the 95th and 5th percentiles of the wind speed distributions, divided by the mean wind speed for that respective period.

4 Discussion and Concluding Remarks

The validation of the Argonne Downscaled Data Archive Version 2 (ADDA-v2) dataset presented in this study underscores its utility in wind resource assessments and climatological applications. This section synthesizes the key findings and compares the performance of ADDA-v2 with ERA5, highlighting ADDA-v2's added value to its coarser resolution forcing data.

ADDA-v2 demonstrated significant advantages over ERA5 in capturing fine-scale wind variability across diverse geographies. The dataset performed particularly well in regions with complex terrain, such as the Rocky Mountains and Alaska, where high-resolution modeling captured localized wind phenomena more effectively. This is especially critical when assessing the consistency in wind power generation throughout the day, with potential implications for hybrid style energy generation. Additionally, ADDA-v2's ability to reduce errors at coarser temporal scales (e.g., weekly and monthly averages) reinforces its applicability for long-term climatological studies and resource planning. However, challenges remain, particularly in regions where both ADDA-v2 and ERA5 struggled, such as the Southeast United States and areas characterized by stable atmospheric conditions. These limitations highlight the need for targeted improvements in existing and new parameterizations (e.g., PBL and LSM) to address specific biases. Additionally, while this validation focused more on inland regions, Sheridan et al. (2025) has evaluated ADDA-v2's performance over coastal locations. Tobias-Tarsh et al. (2025) has evaluated ADDA-v2's performance in wind-related extremes in the context of tropical cyclones over the North Atlantic Basin.

Other studies exist that introduce wind datasets and validate them against observations. For instance, Draxl et al. (2015) documented a 7-year wind dataset with a grid spacing of 2km, primarily focused on wind power evaluations over CONUS and included a limited meteorological validation using 6 tall masts and 3 buoys. Rasmussen et al. (2024) performed validations on a 42-year period, 4km dataset on its near-surface (10m) wind speeds with underestimation especially over complex terrain. While these datasets provide their own unique utility, ADDA-v2 offers a powerful combination of a reasonably long time period with a large spatial domain containing unique geographic regions. By comprehensively validating ADDA-v2's wind speeds and directions using an extensive network of near-surface observations and a diverse set of hub-height observations, this evaluation can provide insight for both climatological studies and wind resource assessments. Yet, all these datasets can be used collectively, complementing one another with their unique characteristics and allowing for a more comprehensive view of model uncertainty and longer-term variability.

However, even with all these datasets developed thus far, it is challenging for high-resolution numerical simulations covering such large domains to capture all model uncertainty and variability. The experiments presented here aim to deliver a relatively robust sample of model uncertainty, but there are many other physics parameterizations that can generate different model solutions. Recent advances in machine-learning (ML) based surrogate model or hybrid model may provide a more comprehensive means of quantifying model uncertainty (Tunnell et al, 2023; Di Santo et al., 2025; Pringle et al. 2025) given faster calculations they can perform.

While this evaluation demonstrates the capabilities of ADDA-v2 in capturing climatological features using multiple metrics over various geospatial locations, some other features can be investigated in future work. One of them is the spatial and temporal variability captured by the model. As demonstrated by past studies (e.g., Müller et al. 2024, Skamarock 2004, and Larsén et al. 2012), atmospheric models with spatial resolution Δx can only capture the energy spectrum at wavelengths ~4-6 Δx. Thus, at a 4km model resolution, the inherent variability and turbulence of the atmosphere can only accurately be simulated at ~20 km scales (Kolmogorov, 1941; Durran, 2010; Skamarock et al., 2008). Evaluation of such variability would require continuous gridded observational data, such as those from radar, lidar or satellites (Müller et al. 2024). Another consideration for future work is to make the evaluations more robust by including multiple model grid cells surrounding each observation site, rather than using only the closest grid cell, as we did in this study. This would allow us to characterize a range of modelled winds around the observation sites and better represent model spatial variability. Lastly, while this study prioritizes climatology inland, future work is needed for analyzing ADDA-v2's capability of capturing extreme winds, which can provide insight into storm-related (e.g., derechos) risk assessments (Li et al. 2025).

Code and Data Availability

All datasets used in this study are freely available, except for the selected proprietary hub-height data. ERA5 reanalysis data is accessible through Climate Data Store: https://cds.climate.copernicus.eu/. ADDA-V2 data is located on the ALCF high-performance storage system and is available upon request; request can be made to cjung2@anl.gov. A subset of the ADDA-v2 dataset is hosted by the National Renewable Energy Laboratory, providing access to hub-height wind speed data (https://developer.nrel.gov/docs/wind/wind-toolkit/wtk-led-climate-v1-0-0-download/). The public in-situ data can be found on Data Archive and Portal (DAP) Platform (https://a2e.energy.gov/data) and the IEM Mesonet (https://mesonet.agron.iastate.edu/ASOS/). Data processing scripts were written in python and can be made available upon request.

Author Contributions

Analysis, software development, and manuscript preparation were performed by KP and JW. Model uncertainty quantification analysis was initiated by JF. Observational data management and processing was performed by LS. The model dataset used in this study was developed by CJ, GS, RK, and CD and post-processed by EY, AP, and AK at hub-heights. All authors were involved in research conceptualization, discussion, and manuscript edits.

Competing Interests

The contact author declares that none of the authors have competing interests.

Acknowledgement

This work has been supported by the Laboratory Directed Research and Development (LDRD) Program at Argonne National Laboratory through the U.S. Department of Energy (DOE) contract DE-AC02-06CH11357 and by the Wind Energy Technologies Office (WETO) of the U.S. Department of Energy Office of Energy Efficiency and Renewable Energy. Computational resources for creating the datasets and for data analysis were provided by the Argonne Leadership Computing Facilities (ALCF) including Theta, and Polaris, and National Renewable Energy Laboratory (NREL)'s High Performance Computers including Eagle and Kestrel. We thank Dr. Larry Berg from Pacific Northwest National Laboratory for his insight into the ensemble design and the analysis at the early stage of this work.

References

Akinsanola, A. A., Jung, C., Wang, J., and Kotamarthi, V. R.: Evaluation of precipitation across the contiguous United States, Alaska, and Puerto Rico in multi-decadal convection-permitting simulations, Scientific Reports, 14, 1, https://doi.org/10.1038/s41598-024-51714-3, 2024.

Carlson, T. N., and Boland, F. E.: Analysis of urban-rural canopy using a surface heat flux/temperature model, Journal of Applied Meteorology, 17, 998–1014, https://doi.org/10.1175/1520-0450(1978)017<0998:AOURCU>2.0.CO;2, 1978.

Carvalho, D., Rocha, A., Gómez-Gesteira, M., and Santos, C.: A sensitivity study of the WRF model in wind simulation for an area of high wind energy, Environmental Modelling and Software, 33, 23–32, https://doi.org/10.1016/j.envsoft.2012.01.019, 2012.

Carvalho, D., Rocha, A., Gómez-Gesteira, M., & Silva Santos, C.: Sensitivity of the WRF model wind simulation and wind energy production estimates to planetary boundary layer parameterizations for onshore and offshore areas in the Iberian Peninsula. Applied Energy, 135. https://doi.org/10.1016/j.apenergy.2014.08.082, 2014.

Chen, T. C., Collet, F., and Di Luca, A.: Evaluation of ERA5 precipitation and 10-m wind speed associated with extratropical cyclones using station data over North America, International Journal of Climatology, 44, 1610–1625, https://doi.org/10.1002/joc.8339, 2024.

Couto, A., and Estanqueiro, A.: Enhancing wind power forecast accuracy using the weather research and forecasting numerical model-based features and artificial neural networks, Renewable Energy, 201, https://doi.org/10.1016/j.renene.2022.11.022, 2022.

Di Santo, D., He, C., Chen, F., and Giovannini, L: ML-AMPSIT: Machine Learning-based Automated Multi-method Parameter Sensitivity and Importance analysis Tool. Geoscientific Model Development, 18, 433–459. https://doi.org/10.5194/gmd-18-433-2025, 2025.

Draxl, C., Hahmann, A. N., Peña, A., and Giebel, G.: Evaluating winds and vertical wind shear from Weather Research and Forecasting model forecasts using seven planetary boundary layer schemes, Wind Energy, 17, 197–216, https://doi.org/10.1002/we.1555, 2014.

Draxl, C., Hodge, B. M., Clifton, A., and McCaa, J.: Overview and meteorological validation of the Wind Integration National Dataset Toolkit, Technical Report NREL/TP-5000-61740, National Renewable Energy Laboratory, Golden, CO, USA, 2015.

Draxl, C., Hodge, B. M., Clifton, A., and McCaa, J.: The Wind Integration National Dataset (WIND) Toolkit, Applied Energy, 151, 355–366, https://doi.org/10.1016/j.apenergy.2015.03.121, 2015.

Draxl, C., et al.: WTK-LED: The WIND Toolkit Long-Term Ensemble Dataset, Technical Report NREL/TP-5000-8845, National Renewable Energy Laboratory. Golden, CO, USA, 2024.

Duplyakin, D., Zisman, S., Phillips, C., and Tinnesand, H.: Bias characterization, vertical interpolation, and horizontal interpolation for distributed wind siting using mesoscale wind resource estimates, Technical Report NREL/TP-2C00-78412, National Renewable Energy Laboratory, Golden, CO, USA, https://doi.org/10.2172/1760659, 2021.

Durran, D. R.: Numerical Methods for Fluid Dynamics: With Applications to Geophysics (2nd ed.). Springer. https://doi.org/10.1007/978-1-4419-6412-0, 2010.

Elliott, D., Schwartz, M., and Scott, G.: Wind Resource Base, in: Encyclopedia of Energy, edited by: Cleveland, C. J., Elsevier, Oxford, UK, https://doi.org/10.1016/B0-12-176480-X/00335-1, 2004.

Gelaro, R., McCarty, W., Suárez, M. J., et al.: The Modern-Era Retrospective Analysis for Research and Applications, Version 2 (MERRA-2). Journal of Climate. https://doi.org/10.1175/JCLI-D-16-0758.1, 2017.

Gensini, V., Haberlie, A.and Ashley., W.: Convection-permitting simulations of historical and possible future climate over the contiguous United States. Climate Dynamics, 60, https://doi.org/10.1007/s00382-022-06306-0, 2022.

Grasu, G., and Liu, P.: Risk assessment of floating offshore wind turbines, Energy Reports, 9, https://doi.org/10.1016/j.egyr.2022.11.147, 2023.

Hahmann, A. N., Vincent, C. L., Peña, A., Lange, J., and Hasager, C. B.: Wind climate estimation using WRF model output: Method and model sensitivities over the sea, International Journal of Climatology, 35, 3232–3247, https://doi.org/10.1002/joc.4217, 2015.

Hawkins, E. and Sutton, R.: The potential to narrow uncertainty in regional climate predictions. Bulletin of the American Meteorological Society, 90(8), pp.1095-1108, https://doi.org/10.1175/2009BAMS2607.1, 2009.

Helbig, N., Mott, R., van Herwijnen, A., Winstral, A., and Jonas, T.: Parameterizing surface wind speed over complex topography, Journal of Geophysical Research: Atmospheres, 122, 2360–2374, https://doi.org/10.1002/2016JD025593, 2017.

Hersbach, H., Bell, B., Berrisford, P., Hirahara, S., Horányi, A., Muñoz-Sabater, J., Nicolas, J., Peubey, C., Radu, R., Schepers, D., Simmons, A., Soci, C., Abdalla, S., Abellan, X., Balsamo, G., Bechtold, P., Biavati, G., Bidlot, J., Bonavita, M., … Thépaut, J. N.: The ERA5 global reanalysis, Quarterly Journal of the Royal Meteorological Society, 146, 1999–2049, https://doi.org/10.1002/qj.3803, 2020.

Hong, S. Y., Noh, Y., and Dudhia, J.: A new vertical diffusion package with an explicit treatment of entrainment processes, Monthly Weather Review, 134, 2318–2341, https://doi.org/10.1175/MWR3199.1, 2006.

Iacono, M. J., Delamere, J. S., Mlawer, E. J., Shephard, M. W., Clough, S. A., and Collins, W. D.: Radiative forcing by long-lived greenhouse gases: Calculations with the AER radiative transfer models, Journal of Geophysical Research: Atmospheres, 113, D13103, https://doi.org/10.1029/2008JD009944, 2008.

Jiménez, P. A., and J. Dudhia: Improving the representation of resolved and unresolved topographic effects on surface wind in the WRF Model. J. Appl. Meteor. Climatol., 51, 300–316, https://doi.org/10.1175/JAMC-D-11-084.1, 2012.

Jones, E., A. A. Wing, and Parfitt, R.: A global perspective of tropical cyclone precipitation in reanalyses. Journal of Climate. https://doi.org/10.1175/JCLI-D-20-0892.1, 2021.

Jung, C., Taubert, D., and Schindler, D.: The temporal variability of global wind energy – Long-term trends and inter-annual variability, Energy Conversion and Management, 188, 68–79, https://doi.org/10.1016/j.enconman.2019.03.072, 2019.

Kayastha, M. B., Huang, C., Wang, J., Pringle W.J., Chakraborty, TC., Yang Z., Hetland, R., Qian Y., and Xue, P. Insights on Simulating Summer Warming of the Great Lakes: Understanding the Behavior of a Newly Developed Coupled Lake-Atmospheric Modeling System. Journal of Advances in Modeling Earth Systems. 15 (7), e2023MS003620, https://doi.org/10.1029/2023MS003620, 2023.

Kolmogorov, A. N.: The local structure of turbulence in incompressible viscous fluid for very large Reynolds numbers, Proceedings of the Royal Society of London. Series A: Mathematical and Physical Sciences, 434(1890), 9–13. https://doi.org/10.1098/rspa.1991.0075, 1941.

Lackmann, G.: Midlatitude Synoptic Meteorology, in: Midlatitude Synoptic Meteorology, edited by: Lackmann, G., American Meteorological Society, Boston, MA, USA, https://doi.org/10.1007/978-1-878220-56-1, 2011.

Lee, J. A., Doubrawa, P., Xue, L., Newman, A. J., Draxl, C., and Scott, G.: Wind resource assessment for Alaska's offshore regions: Validation of a 14-year high-resolution WRF data set. Energies, *12*(14). https://doi.org/10.3390/en12142780, 2014.

Li, H., Claremar, B., Wu, L., Hallgren, C., Körnich, H., Ivanell, S., and Sahlée, E.: A sensitivity study of the WRF model in offshore wind modeling over the Baltic Sea, Geoscience Frontiers, 12, 101229, https://doi.org/10.1016/j.gsf.2021.101229, 2021.

Li, J., Geiss, A., Feng, Z., Leung, L. R., Qian, Y., and Cui, W.: A derecho climatology (2004–2021) in the United States based on machine learning identification of bow echoes, Earth Syst. Sci. Data. https://doi.org/10.5194/essd-2024-112, accepted, 2025.

Liu, C., Ikeda, K., Rasmussen, R., Barlage, M., Newman, A. J., Prein, A. F., Chen, F., Chen, L., Clark, M., Dai, A., Dudhia, J., Eidhammer, T., Gochis, D., Gutmann, E., Kurkute, S., Li, Y., Thompson, G., and Yates, D.: Continental-scale convection-permitting modeling of the current and future climate of North America, Climate Dynamics, 49, 71–101, https://doi.org/10.1007/s00382-016-3327-9, 2017.

Larsén, X. G., Ott, S., Badger, J., Hahmann, A. N., and Mann, J.: Recipes for correcting the impact of effective mesoscale resolution on the estimation of extreme winds, J. Appl. Meteorol. Clim., 51, 521–533, https://doi.org/10.1175/JAMC-D-11-090.1, 2012.

Müller, S., Larsén, X. G., and Verelst, D. R.: Tropical cyclone low-level wind speed, shear, and veer: sensitivity to the boundary layer parametrization in the Weather Research and Forecasting model, Wind Energy. Sci., 9, 1153–1171, https://doi.org/10.5194/wes-9-1153-2024, 2024.

Markowski, P., and Richardson, Y.: Mesoscale Meteorology in Midlatitudes, in: Mesoscale Meteorology in Midlatitudes, edited by: Markowski, P., and Richardson, Y., John Wiley & Sons, Inc., Hoboken, NJ, USA, https://doi.org/10.1002/9780470682104, 2010.

Mesinger, F., DiMego, G., Kalnay, E., et al.: North American Regional Reanalysis. Bulletin of the American Meteorological Society. https://doi.org/10.1175/BAMS-87-3-343, 2006

Millstein, D., Solomon-Culp, J., Wang, M., Ullrich, P., and Collier, C.: Wind energy variability and links to regional and synoptic scale weather, Climate Dynamics, 52, 7–8, https://doi.org/10.1007/s00382-018-4421-y, 2019.

Monin, A. S., and Obukhov, A. M.: Basic laws of turbulent mixing in the surface layer of the atmosphere, Contributions of the Geophysical Institute of the Academy of Sciences of the USSR, 24, 151–157, 1954.

Morrison, H., Curry, J. A., and Khvorostyanov, V. I.: A new double-moment microphysics parameterization for application in cloud and climate models. Part I: Description, Journal of the Atmospheric Sciences, 62, 1665–1677, https://doi.org/10.1175/JAS3446.1, 2005.

Murakami, H.: Tropical cyclones in reanalysis data sets. Geophysical Research Letters. https://doi.org/10.1002/2014GL059519, 2014

Nakanishi, M., and Niino, H.: Development of an improved turbulence closure model for the atmospheric boundary layer, Journal of the Meteorological Society of Japan, 87, 895–912, https://doi.org/10.2151/jmsj.87.895, 2009.

Niu, G. Y., Yang, Z. L., Mitchell, K. E., Chen, F., Ek, M. B., Barlage, M., Kumar, A., Manning, K., Niyogi, D., Rosero, E., Tewari, M., and Xia, Y.: The community Noah land surface model with multiparameterization options (Noah-MP): 1. Model description and evaluation with local-scale measurements, Journal of Geophysical Research: Atmospheres, 116, D12109, https://doi.org/10.1029/2010JD015139, 2011.

Powers, J. G., Klemp, J. B., Skamarock, W. C., Davis, C. A., Dudhia, J., Gill, D. O., Coen, J. L., Gochis, D. J., Ahmadov, R., Peckham, S. E., Grell, G. A., Michalakes, J., Trahan, S., Benjamin, S. G., Alexander, C. R., Dimego, G. J., Wang, W., Schwartz, C. S., Romine, G. S., … Duda, M. G.: The weather research and forecasting model: Overview, system efforts, and future directions, Bulletin of the American Meteorological Society, 98, 1717–1737, https://doi.org/10.1175/BAMS-D-15-00308.1, 2017.

Prein, A. F., Langhans, W., Fosser, G., Ferrone, A., Ban, N., Goergen, K., Keller, M., Tölle, M., Gutjahr, O., Feser, F., Brisson, E., Kollet, S., Schmidli, J., van Lipzig, N. P. M., and Leung, R.: A review on regional convection-permitting climate modeling: Demonstrations, prospects, and challenges, Reviews of Geophysics, 53, 323–374, https://doi.org/10.1002/2014RG000475, 2015.

Pringle, W. J., Huang, C., Xue, P., Wang, J., Sargsyan, K., Kayastha, M. B., Chakraborty, T. C., Yang, Z., Qian, Y., and Hetland, R. D. Coupled Lake-Atmosphere-Land Physics Uncertainties in a Great Lakes Regional Climate Model. DOI: 10.1029/2024MS004337. Journal of Advances in Modelling Earth Systems, 2025.

Pryor, S. C., Shepherd, T. J., and Barthelmie, R. J.: Interannual variability of wind climates and wind turbine annual energy production, Wind Energy Science, 3, 651–672, https://doi.org/10.5194/wes-3-651-2018, 2018.

Rasmussen, R. M., Chen, F., Liu, C. H., Ikeda, K., Prein, A., Kim, J., Schneider, T., Dai, A., Gochis, D., Dugger, A., Zhang, Y., Jaye, A., Dudhia, J., He, C., Harrold, M., Xue, L., Chen, S., Newman, A., Dougherty, E., … Miguez-Macho, G.: CONUS404 The NCAR–USGS 4-km long-term regional hydroclimate reanalysis over the CONUS, Bulletin of the American Meteorological Society, 104, 105182, https://doi.org/10.1175/BAMS-D-21-0326.1, 2023.

Scott, D. W.: Multivariate density estimation: Theory, practice, and visualization, 2nd ed., John Wiley & Sons, Inc., Hoboken, NJ, USA, https://doi.org/10.1002/9781118575574, 2015.

Sheridan, L. M., Krishnamurthy, R., Gorton, A. M., Shaw, W. J., and Newsom, R. K.: Validation of reanalysis-based offshore wind resource characterization using lidar buoy observations. Marine Technology Society Journal. https://doi.org/10.4031/MTSJ.54.6.13, 2020.

Sheridan, L. M., et al.: Offshore reanalysis wind speed assessment across the wind turbine rotor layer off the United States Pacific coast. Wind Energy Science (Online). https://doi.org/10.5194/wes-7-2059-2022, 2022.

Sheridan, L. M., et al.: Validation of wind resource and energy production simulations for small wind turbines in the United States. Wind Energy Science (Online). https://doi.org/10.5194/wes-7-659-2022, 2022.

Sheridan, L. M., Wang, J., Draxl, C., Bodini, N., Phillips, C., Duplyakin, D., Tinnesand, H., Rai, R. K., Flaherty, J. E., Berg, L. K., Jung, C., and Young, E.: Performance of wind assessment datasets in United States coastal areas, Wind Energy Science, https://doi.org/10.5194/wes-2024-115, 2025.

Skamarock, W. C., Klemp, J. B., Dudhia, J., Gill, D. O., Barker, D. M., Duda, M. G., Huang, X.-Y., Wang, W., and Powers, J. G.: A description of the Advanced Research WRF Version 3 (NCAR Technical Note NCAR/TN–475+STR). Boulder, CO: National Center for Atmospheric Research. https://doi.org/10.5065/D68S4MVH, 2008.

Skamarock, W. C., and Coauthors: A description of the Advanced Research WRF version 4. NCAR Tech. Note NCAR/TN-5561STR, 145 pp., http://doi.org/10.5065/1dfh-6p97, 2019.

Skamarock, W. C., Klemp, J. B., Dudhia, J. B., Gill, D. O., Barker, D. M., Duda, M. G., Huang, X.-Y., Wang, W., and Powers, J. G.: A Description of the Advanced Research WRF Model Version 4.3, NCAR Technical Note, TN-556+STR, National Center for Atmospheric Research, Boulder, CO, USA, 2021.

Skamarock, W. C.: Evaluating mesoscale NWP models using kinetic energy spectra, Mon. Weather Rev., 132, 3019–3032, https://doi.org/10.1175/MWR2830.1, 2004

Tewari, M., Chen, F., Wang, W., Dudhia, J., LeMone, M. A., Mitchell, K., Ek, M., Gayno, G., Wegiel, J., and Cuenca, R. H.: Implementation and verification of the unified Noah land surface model in the WRF model, Bulletin of the American Meteorological Society, 85, 1361–1363, https://doi.org/10.1175/BAMS-85-10-1361, 2004.

Tobias-Tarsh, L., Jung, C., Wang, J., Bobde, V., Akinsanola, A. A., and Kotamarthi, V. R.: Evaluation of North Atlantic Tropical Cyclones in a Convection-Permitting Regional Climate Simulation, EGUsphere [preprint], https://doi.org/10.5194/egusphere-2025-1805, 2025.

Tunnell, M., Bowman, N., and Carrier, E.: Fast Gaussian process emulation of Mars Global Climate Model. Earth and Space Science, 10, e2022EA002743, https://doi.org/10.1029/2022EA002743, 2023.

Wang, C., and Jin, S.: Error features and their possible causes in simulated low-level winds by WRF at a wind farm, Wind Energy, 17, 1415–1427, https://doi.org/10.1002/we.1635, 2014.

Wang, J., & Kotamarthi, V. R.: Downscaling with a nested regional climate model in near-surface fields over the contiguous United States. Journal of Geophysical Research, *119*(14). https://doi.org/10.1002/2014JD021696, 2014.

Wang, C., & Jin, S.: Error features and their possible causes in simulated low-level winds by WRF at a wind farm. Wind Energy, *17*(9). https://doi.org/10.1002/we.1635, 2014.

Wang, J., Bessac, J., Kotamarthi, R., Constantinescu, E., and Drewniak, B.: Internal variability of a dynamically downscaled climate over North America, Climate Dynamics, 50, 4341–4364, https://doi.org/10.1007/s00382-017-3889-1, 2018.

Wilczak, J. M., Akish, E., Capotondi, A., and Compo, G. P.: Evaluation and bias correction of the ERA5 reanalysis over the United States for wind and solar energy applications, Energies, 17, 1667, https://doi.org/10.3390/en17071667, 2024.

Wu, C., Luo, K., Wang, Q., and Fan, J.: Simulated potential wind power sensitivity to the planetary boundary layer parameterizations combined with various topography datasets in the weather research and forecasting model, Energy, 239, 122047, https://doi.org/10.1016/j.energy.2021.122047, 2022.

Wu, Q., Bessac, J., Huang, W., Wang, J., and Kotamarthi, R.: A conditional approach for joint estimation of wind speed and direction under future climates, Advances in Statistical Climatology, Meteorology and Oceanography, 8, 205–218, https://doi.org/10.5194/ascmo-8-205-2022, 2022.

Yang, B., Qian, Y., Berg, L. K., Ma, P. L., Wharton, S., Bulaevskaya, V., Yan, H., Hou, Z., and Shaw, W. J.: Sensitivity of turbine-height wind speeds to parameters in planetary boundary-layer and surface-layer schemes in the Weather Research and Forecasting Model, Boundary-Layer Meteorology, 162, 117–139, https://doi.org/10.1007/s10546-016-0185-2, 2017.